eLife

Reviewed Preprint
v1 • June 1, 2026
Not revised

For correspondence:
yangyingchun@xiyi.edu.cn
yuzhaoxiang@xiyi.edu.cn
lbzhang@nwpu.edu.cn

Competing interests: No competing interests declared

Funding: See page 26

Reviewing editor: Marcelo A Mori, Universidade Estadual de Campinas (UNICAMP), Brazil

Photo-downregulation of SIRT4 mitigates aging in mice by enhancing H3K9ac via fatty acid metabolism

Fangqing Deng[1], Rong Yang[1], Xu Li[1], Jinyun Niu[1], Zibo Gao[1], Monian Wang[1], Yang Liu[1], Lihua Yang[1], Huifang Liu[1], Yingchun Yang[2] ✉, Zhaoxiang Yu[2] ✉, Lianbing Zhang[1] ✉

[1]School of Life Science and Technology, Northwestern Polytechnical University, Xi'an, China • [2]The First Affiliated Hospital of Xi'an Medical University, Xi'an, China

eLife Assessment

This potentially **valuable** study investigates the anti-senescence effects of red light exposure, proposing that reduced SIRT4 levels enhance fatty acid metabolism and H3K9ac, thereby attenuating ageing-related phenotypes. The authors use multiple approaches, including cultured cells, animal models, and molecular analyses, to support their conclusions. However, the evidence remains **incomplete**, as additional controls and stronger mechanistic data are needed to fully support the proposed pathway, particularly how red light exposure reduces SIRT4 levels.

https://doi.org/10.7554/eLife.111498.1.sa3

Abstract

As organisms age, mitochondrial metabolic activity declines, and disrupted gene expression regulation mediated by histone acetylation induces the emergence of senescent physiological phenotypes in tissues. In this study, we found that periodic exposure to red light significantly increased histone H3 Lys9 acetylation (H3K9ac) levels in the tissues and organs of aged mice. Following red light exposure, silent information regulation factor 4 (SIRT4) protein levels in keratinocytes were notably reduced, whereas glycolysis, fatty acid metabolism, and the tricarboxylic acid (TCA) cycle were significantly activated in keratinocytes. The reduction in mitochondrial SIRT4 levels enhances the acetylation of mitochondrial metabolic proteins, particularly malonyl-CoA decarboxylase (MCD), a potent inhibitor of the key rate-limiting enzyme carnitine palmitoyltransferase 1A (CPT1A) in fatty acid oxidation. This process promotes mitochondrial fatty acid oxidation and TCA cycle. Additionally, the decrease in SIRT4 activates SIRT1 through feedback mechanisms, thereby alleviating its inhibition on PPAR-α in senescent keratinocytes and comprehensively activating the expression of genes related to lipid metabolism. This lipid metabolism activation ultimately facilitates the accumulation of acetyl-CoA within keratinocytes, increases H3K9ac levels, and reshapes the expression patterns of senescence-related genes. Eventually, cellular aging is effectively mitigated by the synergistic regulation of metabolism, inflammation, and gene expression.

Graphical Abstract

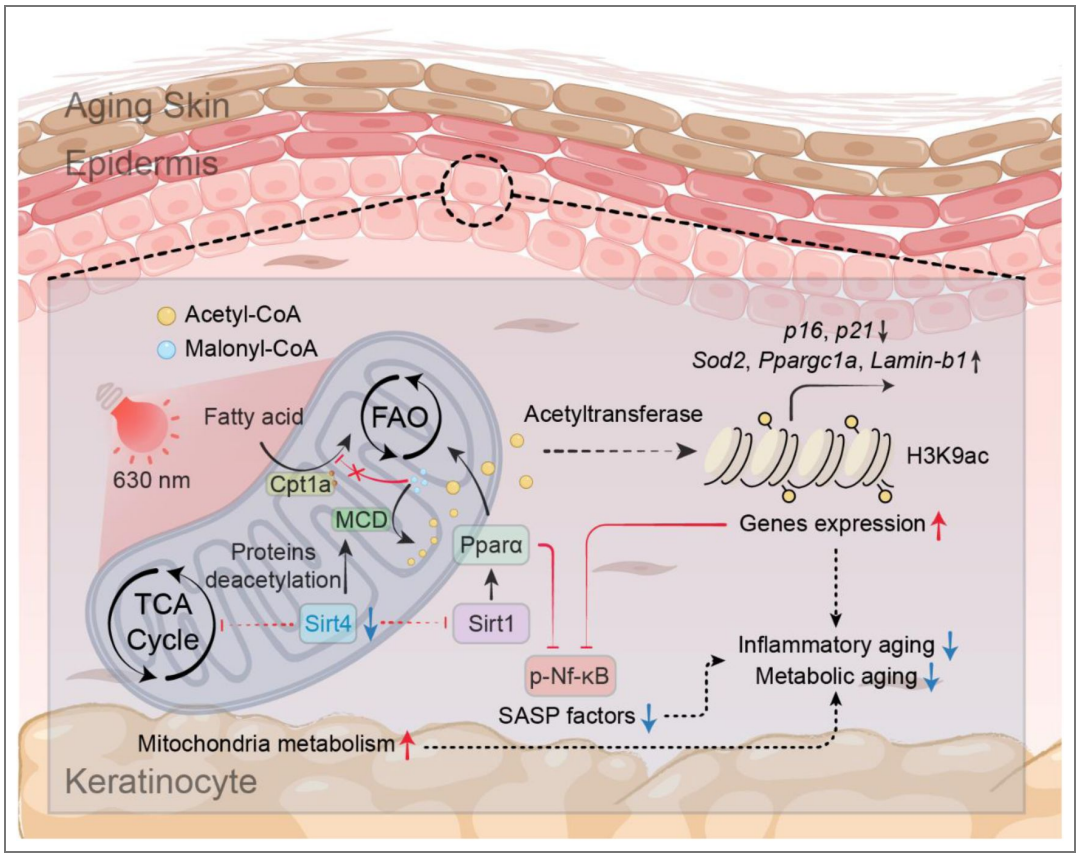

Mechanism of anti-aging action of red light. Red light can reduce SIRT4 signalling in keratinocytes, thereby reactivating lipid metabolism and increasing levels of acetyl-CoA. This promotes histone acetylation, which in turn reverses the expression of age-related inflammatory factors and genes.

Introduction

Aging is characterized by the onset of chronic inflammation, cardiovascular fibrosis, subcutaneous melanin accumulation, wrinkle formation, and other physiological changes[1, 2]. These alterations pose significant risks to the physical and mental wellbeing of the elderly population[3]. Therefore, it is crucial to thoroughly investigate the mechanisms of aging and develop comprehensive anti-aging strategies and interventions.

Existing research has elucidated the mechanism by which histone acetylation influences aging phenotypes through genomic expression regulation[4]. Changes in the acetylation levels at age-related histone acetylation sites directly shape cellular and tissue aging phenotypes[5, 6]. For example, elevated levels of H3K9ac, H3K56ac, and H3K27ac maintain chromatin accessibility, enhance binding of relevant transcription factors, and not only upregulate antioxidant genes (*SOD2*, *NRF2*) to suppress NF-κB-mediated inflammatory signaling and SASP aging factor secretion[7–11], but also directly inhibit promoters of cell cycle suppressors ($P16^{INK4a}$, $P21^{CIP1}$)[12–14]. As a key metabolite and the sole substrate for histone acetylation, acetyl-CoA links cellular metabolic states to senescence phenotypes through histone acetylation[4, 15]. Under the influence of intracellular acetyltransferase and deacetylase systems, increased or decreased cellular metabolism affects histone acetylation levels by regulating acetyl-CoA content[16, 17]. This pattern of gene expression, regulated by metabolism and histone acetylation during cellular aging, provides a strategy for delaying aging phenotypes. Specifically, by increasing cellular metabolism or inhibiting histone deacetylase activity, the modification of senescence-associated histone acetylation sites can be enhanced to delay cellular senescence[18–20].

Protein acetylation levels are regulated by deacetylases and acetyltransferases[21–23]. The activities of these enzymes are closely linked to the metabolic state of the cell[4]. In particular, with respect to protein deacetylases, three major classes of histone deacetylases (HDACs) have been identified within cells[22]. Class I and Class II HDACs are both Zn^{2+}-dependent and primarily localized to the nucleus[24]. Class III HDACs comprise the NAD^+-dependent Sirtuins (SIRT1-SIRT7) family proteins, which exhibit diverse localization patterns and possess deacetylase activity[25, 26]. Notably, Sirtuins deacetylate not only histones but also numerous non-histones, including transcription factors, metabolic enzymes, and DNA repair proteins, playing central roles in regulating metabolism, stress resistance, genomic stability, inflammation, and aging[27–29]. Among these Sirtuins, SIRT7 is expressed in the nucleolus and directly regulates ribosomal transcription, making it a key gene for cellular survival[28, 30]. While studies have clearly demonstrated that overexpression of SIRT1/6 extends lifespan in model organisms and that SIRT3/6 deficiency causes severe premature aging in mice, the anti-aging mechanisms of SIRT4/5 remain incompletely understood[30–35]. In calorie-restriction experiments, SIRT4 activity was suppressed, suggesting that SIRT4 may serve as potential feedback regulators of Sirtuins[30]. Unlike Class I and Class II HDACs, Sirtuins exhibit NAD^+ dependence. Consequently, current anti-aging strategies targeting sirtuins primarily focus on elevating NAD^+ levels (through supplementation of NAD^+ precursors such as NMN/NR) or employing sirtuin-specific activators, which are currently popular anti-aging interventions[36].

Red light exerts potent intrinsic regulatory effects on metabolism. As an environmental stimulus, red light mediated photobiomodulation is characterized primarily by the enhancement of cellular metabolism and mitigation of inflammation[37–39]. In clinical settings, visible red light is routinely employed to accelerate metabolic activity in hair follicles and treat diverse cutaneous inflammatory responses[38, 40, 41]. As a noninvasive intervention, the effects of red light have also garnered public interest through devices such as ‘photorejuvenation devices’ and ‘home wearable wound light care,’ which have yielded significant social and economic benefits, underscoring their efficacy in skin repair and potential for anti-aging applications[42–45]. Notably, the metabolic remodeling capacity of red light implies a potential link to the regulation of histone acetylation. However, the relationship between red light-driven metabolic regulation and histone acetylation, as well as the mechanism by which red light regulates histone acetylation, remain unclear. We sought to understand how red light exerts these beneficial effects through the regulation of histone acetylation and its specific molecular mechanisms. Therefore, we irradiated aging mouse and cell models with red light and monitored changes in aging-related physiological indicators post-treatment to explore the potential of red light for epigenetic modification and antiaging effects.

In our study, we found that periodic exposure to red light significantly increased H3K9ac levels in the tissues and organs of aged mice. Following red light exposure, SIRT4 protein levels in keratinocytes were notably reduced, while glycolysis, fatty acid metabolism, and the tricarboxylic acid (TCA) cycle were significantly activated. Further mechanistic investigations suggested that the reduction in mitochondrial SIRT4 levels enhances the acetylation of mitochondrial metabolic proteins, particularly malonyl-CoA decarboxylase (MCD), a potent inhibitor of the key rate-limiting enzyme carnitine palmitoyltransferase 1A (CPT1A) in fatty acid oxidation. This process promotes mitochondrial fatty acid oxidation and TCA cycle activity. Additionally, the decrease in SIRT4 activates SIRT1 through feedback mechanisms, thereby alleviating its inhibition on PPAR-α in senescent keratinocytes and comprehensively activating the expression of genes related to lipid metabolism. This lipid metabolism activation ultimately facilitates the accumulation of acetyl-CoA within keratinocytes, increases H3K9ac levels, and reshapes the expression patterns of senescence-related genes. Consequently, it mitigates the dysregulation of genomic expression and excessive inflammatory activation associated with cellular senescence. Ultimately, cellular aging is effectively mitigated through the synergistic regulation of metabolism, inflammation, and genomic expression. In a word, our study reveals a novel anti-aging intervention strategy targeting SIRT4 downregulation to increase H3K9ac levels. We propose that controlling the abnormal age-related activation of SIRT4 during cellular senescence and developing SIRT4 inhibitors may enable tissue-specific senescence reversal and therapeutic interventions for metabolic diseases.

Methods

Cell culture and animal models

PAM212 (Cat. No. MZ-2610) cell lines were purchased from Ningbo Mingzhou Biotechnology Co., Ltd. Under non-experimental conditions, the cells were maintained in Dulbecco's Modified Eagle's medium (DMEM, C11995500BT, Gibco, USA). containing 10% (v/v) fetal bovine serum (FBS), 100 U/mL penicillin, and 100 mg/mL streptomycin. Prior to red light irradiation treatment, the old medium was removed, the cells were carefully rinsed with D-PBS, and the medium was replaced with phenol red-free DMEM. For both irradiation and maintenance cultures, the cells were placed in a cell culture incubator, and the temperature of the incubator was maintained at 37 °C, 80% humidity, and 5% CO2.

SPF-grade female C57BL/6 mice (4–5 weeks) were purchased from Xi'an Keao Biotechnology Co., Ltd. The mice used in this study were housed in a dedicated experimental microbarrier (HH-MMB-1, Monkey Animal Experimental Equipment Technology Co., Ltd., Suzhou, China) and provided with an unrestricted standard laboratory diet and water. The microbarrier temperature was maintained at 26 °C. When the mice reached the age of 8 months, periodic red light irradiation treatments were performed according to the light treatment protocol for mice in this study. Red-light-irradiated mice were analyzed at the end of treatment. All animal experiments involved in this study were approved by the Animal Ethics Committee of Northwestern Polytechnical University (Ethics No. 202401023).

Model of keratinocyte senescence

2×10^5 PAM212 cells were seeded in 6-well plates and incubated overnight in a cell culture incubator. When the cell confluency reached 50%-60%, the medium was removed, and 2 mL of PBS was added to rinse the cells. After replacing the serum-free medium with H_2O_2 at a concentration of 300 μM, the cells were returned to the cell culture incubator and treated for 2 h to induce premature senescence following oxidative stimulation. After H_2O_2 treatment, the old medium was removed, the cells were rinsed twice with 2 mL of PBS, and the complete medium was replaced and incubated for 72 h. During this period, the fluid was changed, and treatments were added according to the actual conditions. Cellular senescence was detected using SA-β-Gal staining.

Lighting equipment and light treatment solutions

The light source used in this study was purchased from Xuzhou Aijia Electronic Science and Technology Co., Ltd., and had a rated power of 12 W. The light source was emitted by LEDs, and 96 LEDs were distributed on a planar light plate according to the standard wells of a 96-well cell culture plate. The wavelength range of the LED light source was 625 nm-635 nm. The cells and mice were irradiated in an opaque darkroom with a bottom area of 400 cm^2, and the power density of red light received at the bottom plane of the darkroom was 0.03 J/(cm^2·s) under rated power operating conditions. For the red light irradiation source employed in this study, the distance from the irradiation plane of the mouse (the dorsal skin of the mouse) was 10 cm, and the distance from the irradiation plane of the keratinocytes was 15 cm. In this study, four irradiation dose gradients of 0 J/cm^2, 40 J/cm^2, 80 J/cm^2 and 160 J/cm^2 were used to treat cells and mice. The irradiation treatment times for the four dose gradients were 0, 1333, 2667, and 5333 s. The irradiation treatment of the cells was carried out in a cell incubator, and the irradiation treatment experiments were conducted in a low-light, room-temperature environment. Details of the light treatments are provided in the Supplementary Material (Fig. S1). Unless otherwise specified, the cellular treatment dose was set at 80 J/cm^2.

Red light irradiation of senescent mice was performed according to the following procedure: C57BL/6 mice aged 8 months were used, and all hair on the backs of the mice was removed using a depilatory cream prior to irradiation. The mice were then subjected to continuous red light treatment according to a treatment cycle of 15 days of red light treatment every two months.

During each treatment cycle, the mice were irradiated with red light at a dose of 80 J/cm^2 once daily for 15 days. Mice in the control group were subjected to the same dehairing treatment but were not red-light irradiated. Red-light-treated model mice and normal senescent mice reaching 1 and 2 years of age were euthanized with an overdose of sodium pentobarbital, and tissue samples from these senescent mice were collected for the analysis of senescence indices and related experiments. All senescent mice used in this study were female.

RNA Sequencing and Transcriptome Analysis

2×10^6 PAM212 in 10 cm cell culture plates with 80% cell fusion was replaced with phenol red-free DMEM medium, and then treated with red light irradiation to expose them to red light irradiation at a dose of 80 J/cm^2. The control group underwent the same fluid change operation without any irradiation. The number of biological replicates was set to n=3. After irradiation, the cells were cultured in an incubator for 12 h. The cells were then collected using a cell scraper, centrifuged to obtain a cell precipitate, and snap frozen in liquid nitrogen. After extracting cellular RNA, the transcripts of red light-irradiated PAM212 cells were sequenced by Sangon Biotech (Shanghai) Co., Ltd. The raw image data files obtained using Illumina HiSeq™ were converted into raw sequencing sequences using CASAVA Base Calling Analysis, and the sequencing sequences were assessed for quality using FastQC. Quality-assessed transcripts were used for genome structure, expression level, differential expression, and gene enrichment analyses, and the results of the differential analysis were plotted and visualized.

Proteomics and acetylated proteomics analysis

The same cell processing procedure used for transcriptome sequencing analysis was used to treat keratinocytes. After red light irradiation, the keratinocytes were cultured in an incubator for 24 h. Keratinocytes were collected by cell scraping, centrifuged to obtain a cell precipitate, and snap-frozen in liquid nitrogen. Total cell protein was extracted (n=3, the number of keratinocytes in each sample was more than 5×10^7), and the total protein of keratinocytes treated with red light irradiation was obtained from Shanghai Oebiotech Co., Ltd. for proteomic analysis and acetylation modification. After the extracted proteins were enzymatically digested, LC-MS/MS was used to identify the digested peptides, and the mass spectrometry data of each sample were collected in combination with DIA for spectral matching and proteomic library construction. For acetylated proteins, acetylated peptides were first enriched by acetylation, and then the library was constructed using LC-MS/MS (4D-DIA). After library construction, the peptides were processed for the analysis of differentially expressed proteins and differentially acetylated proteins after quality control. The results of the proteomics and acetylation-modified proteomics difference visualization analyses were plotted by comparing the data of the differentially expressed proteins in the GO and KEGG databases.

Real-time Quantitative Polymerase Chain Reaction

RNA was extracted using the FastPure Cell/Tissue Total RNA Isolation Kit (RC113-01, Vazyme Biotech, China). For PAM212 cells, after removing the culture medium, the cells were covered with lysate (500 μl buffer SRL for every 2×10^6 cells), and the cell lysate was collected to extract RNA, according to the manufacturer's instructions. The tissues were then frozen in liquid nitrogen and ground into a powder. A total of 20 mg of animal tissue was collected and added to 500 μL buffer SRL, and RNA was extracted according to the manufacturer's instructions. RNA concentration was determined using a Nanodrop (NanoDrop One, Thermo Fisher, USA) after obtaining RNA. A total of 500 ng of RNA was extracted from each sample and reverse-transcribed using ABScript III RT Master Mix (RK20429, Abclonal, China) for qPCR. Finally, real-time quantitative PCR was used to detect differences in gene expression between the groups. The QPCR instrument was purchased from Bioer Technology Co., Ltd. (FQD-96A, Bioer Technology, China). Primers used for qPCR were listed in Supplementary Table S1.

Western blot

Treated PAM212 cells or liquid nitrogen snap-frozen and ground animal tissue samples were added to an appropriate amount of RIPA lysate (ZG394617, Thermo Fisher, USA, 100 μl RIPA lysis buffer per 1 × 10^6 cells or 600 μl RIPA lysis buffer per 20 mg animal tissue) to extract the total protein. Lysis was performed on ice for 30 min, during which the cells were vortexed and shaken for 10 s every 10 min. The samples were centrifuged for 15 min at 4°C and 12,000 × g. The supernatant (total protein) was aspirated into a new EP tube. The total protein concentration of the protein samples was determined using the BCA assay (P1511, Beijing Applygen Gene Technology, China). All samples were adjusted to the same concentration using RIPA lysate, and 5× SDS-PAGE buffer (RM00001, Abclonal, China) was added to each sample. The proteins were denatured by boiling in a water bath for 10 min. Sampling was performed using a gradient precast gel (ET12420Gal, ACE Biotechnology, China) from ACE Biotechnology Co., Ltd., and the sample volume was 10-20 μg of protein. Electrophoresis (constant voltage of 120 V for approximately 60–90 min) was performed using an electrophoresis chamber (PowerPac Basic, Bio-Rad, USA). Membrane transfer was performed using a rapid membrane transfer apparatus (PB0010, Thermo Fisher, USA). Polyvinylidene fluoride (PVDF, #1620177, Bio-Rad, USA) membranes were purchased from Bio-Rad Laboratories Inc. After transfer, the PVDF membranes were blocked using a rapid blocking solution from New Cell & Molecular Biotech Co.,Ltd. The PVDF membranes were then incubated with the following primary antibodies: NF-κb (A22331, Abclonal, China), p-NF-κB (AF5875, Beyotime, China), IκB-α (A19714, Abclonal, China), Actin (AC026, Abclonal, China), LMNB1 (A1910, Abclonal, China), P16 (A24653, Abclonal, China), P21 (A27846, Abclonal, China), p-mTOR (AP0094, Abclonal, China), Glut1 (A6982, Abclonal, China), PI3K (A22467, Abclonal, China), p-AKT1 (AA329, Beyotime, China), PPAR-α (A22887, Abclonal, China), PPAR-γ (GB11164, Servicebio, China), H3K9ac (A21107, Abclonal, China), H3K4ac (A24340, Abclonal, China), H3K27ac (F0271, Selleck, USA), H3-K9/K14/K18/K23/K27ac (A17917, Abclonal, China), H3 (A2348, Abclonal, China), mTORC1 (A8992, Abclonal, China), mTORC2 (27248-1-AP, Proteintech, China), p-S6 (AP1471, Abclonal, China), SIRT1 (A17307, Abclonal, China), SIRT3 (A7307, Abclonal, China), SIRT4 (A7585, Abclonal, China), and Tubulin (A12289 Abclonal, China). After incubating the membrane with the primary antibody solution at 4 °C overnight (12-16 h), the membrane was washed six times with TBST for 5 min each. The membrane was then incubated with an HRP-labelled secondary antibody of the corresponding species at room temperature for 1 h. Finally, the membrane washing operation was repeated, an appropriate amount of ECL luminescent solution was added to the PVDF membrane, and the signals of the target bands were captured using a gel-imaging system.

Mitochondrial membrane potential assay (JC-1)

3 × 10^4 PAM212 cells were seeded in 35 mm confocal specialized culture dishes, and overnight adherence was continued until cell fusion reached 50-60%. After red light treatment of PAM212 cells, changes in the mitochondrial membrane potential in keratinocytes were detected using the Enhanced Mitochondrial Membrane Potential Assay Kit (C2003S, Beyotime Biotechnology, China). Ltd. Membrane potential collapse was induced by adding CCCP (10 μM) for 20 min to the positive-control group. The JC-1 probe working solution (5 μM) was prepared in a serum-free medium and added to the experimental and control groups. The medium was removed from the Petri dishes, and 1 mL of preformulated JC-1 working solution was added and incubated for 20 min at 37°C in the dark. The cells were gently washed with pre-warmed JC-1 Wash Buffer (provided in the kit) 3 times for 5 min each. Phenol Red-free medium (1 mL) containing 10% FBS was added, and fluorescence imaging was performed using a confocal microscope (SP8, Leica, Germany). Microplate reader detection was performed in a 96-well plate, and staining was performed as described above. The optical density (OD) values of the different treatment groups at 488 nm (monomers, green) and 561 nm (aggregates, red) were determined.

Cell activity, migration and proliferation assays

Changes in cell viability were detected using the CCK-8 assay (C6005, NCM Biotech, China) after treating the cells with red light irradiation. 5×10^3 PAM212 cells were seeded in 96-well plates, and the medium was changed to phenol red-free complete DMEM after overnight wall attachment. The keratinocytes were treated with red light irradiation, and 10 μl of CCK-8 solution was added to each well after red light treatment. The OD value of the cell cultures at 450 nm was measured using a microplate reader after incubation at 37 ℃ for 1 h.

Changes in the migration ability of the cells were detected using a Wound Healing Assay. PAM212 cells (10^6) were seeded in 6-well plates and incubated at 37 °C until a 90%-100% cell fusion rate was achieved. The cell layer was scraped vertically using a sterile 200 μl pipette tip to form a straight line of scratches. The cells were then gently rinsed three times with PBS to remove the shed cells, and the medium was replaced with phenol red-free DMEM containing 1% FBS. The initial state of the scratch at 0 h was recorded using an optical microscope. The cells were treated with red light irradiation, and the scratch was photographed again at the same location after 24 h of cell migration to observe the filling of the scratch by cell migration.

Changes in cell proliferative capacity were detected by cell counting. After inoculation of 2×10^5 PAM212 cells in 6-well plates and overnight culture, the phenol red-free medium was changed, and the cells were irradiated with red light. Adherent PAM212 cells were digested with trypsin and collected at 0h, 6h, 12h, 18h, and 24h after the end of red light treatment. The number of PAM212 cells in the control and red light-treated groups at these time points was counted using a cell counter (Countstar Mira BF, Shanghai Ruiyu Biotech Co., Ltd., China).

Chromatin immunoprecipitation–qPCR

Chromatin immunoprecipitation (ChIP) was performed using the Chromatin Immunoprecipitation Kit (RK20258, Abclone, China) according to the manufacturer's instructions. Purified DNA samples obtained from immunoprecipitation reactions were employed in quantitative PCR (qPCR) reactions using a DNA purification kit (RK30100, Abclone, China). ChIP-qPCR primers are listed in Supplementary Table S2.

Metabolite detection laboratory

After the cells were treated with red light irradiation, the intracellular levels of glucose, lactate, triglycerides, fatty acids, and pyruvate were detected using metabolite assay kits produced by Beyotime Biotechnology Co., Ltd. 2×10^6 PAM212 cells were seeded in a 10 cm cell culture dish and cultured until cell confluency reached 80%. The medium was replaced with phenol red-free DMEM, and the cells were irradiated with graded doses of red light. After irradiation, the cells were digested with trypsin and counted at 0h and 12h after irradiation. After counting, the cell precipitates were collected, and the levels of the corresponding metabolites in the cells at 0 and 12 h after exposure to different doses of red light were detected according to the metabolite extraction and assay procedure of the corresponding metabolite assay kits.

NADPH, NADH and GSH content test

The 2×10^6 PAM cells precipitates were collected according to the cell treatment and sample collection procedure in the metabolite assay experiment, and the content of NADPH, NAD^+, and NADPH+NAD^+ in the cells after red light treatment was measured using an NADPH assay kit (S0179, Beyotime Biotechnology, China). Similarly, NADH, NAD^+, and NADH + NAD^+ levels in the red light-treated cells were measured using an NADH assay kit (S0176S, Beyotime Biotechnology, China). The GSH and GSSG contents in the cells after red light treatment were measured using a GSH content assay kit (S0053, Beyotime Biotechnology, China).

Detection of ATP content

The effects of different doses of red-light irradiation on cellular ATP production after cell treatment were determined using an ATP content assay kit (S0027, Beyotime Biotechnology, China). Ltd. Immediately after red light irradiation, cell lysate (200 μl per well of a 6-well plate provided in the kit) was added to the Petri dish and lysed on ice for 5 min. The cell lysate was collected, centrifuged at 12000 × g for 5 min at 4 °C, and the cell supernatant was collected. Next, 20 μL of the cell supernatant to be tested and 100 μL of ATP assay working solution were added to an opaque black 96-well plate, and 560 nm emitted light was detected using a multimode microplate reader (SpectraMax M5, Molecular Devices, USA). The total protein concentration in the sample was determined simultaneously using the BCA method: ATP content (nmol/mg protein) = sample ATP concentration/protein concentration.

β-Galactosidase staining

Senescent cells were stained for galactosidase using a β-galactosidase Staining Kit (G1125-100ML, Servicebio, China) from Wuhan Servicebio Technology Co., Ltd. The cell culture medium was removed from the treated cells in 6-well plates, the cells were washed twice with PBS, 1 mL of β-galactosidase staining fixative was added, and the cells were fixed at room temperature for 15 min. The cells were rinsed three times with PBS for 2 min each, incubated with β-galactosidase staining working solution, and incubated overnight at 37 °C. The cells were observed under a microscope, and images of the galactosidase staining were captured.

Cell immunofluorescence assay

2×10^4 PAM212 cells were seeded onto confocal focusing dishes, allowed to adhere overnight, and cultured until 50%-60% cell fusion. The cells were treated with red light and incubated for 12 h. The medium was removed, and the cells were washed twice with PBS. Cells were then fixed with 4% paraformaldehyde for 15 min at room temperature and washed with PBS three times for 5 min each. PAM212 cells were permeabilized for 10 min at room temperature using an immunostaining permeabilizing solution (P0095, Beyotime Biotechnology Co. Ltd, China), and the PBS washing step was repeated. The blocking solution was added and incubated at 37 °C for 2 h, after which it was removed and incubated with a primary antibody. The primary antibodies (Sirt4, PPAR-α, p16, and H3K9ac) were diluted 1:100-1:200 and incubated overnight at 4 °C according to the actual conditions. The washing step was repeated, and the cells were incubated with a fluorescent secondary antibody (FITC/Cy3, 1:200) produced by Wuhan Abclonal Biotech Co., Ltd for 1h in the dark at 37 °C under a seal. After removing the secondary antibody, the cells were stained with 10 μM DAPI (BL105A, Biosharp, China) for 5 min and washed again after removing the DAPI staining solution. Finally, a fluorescent anti-quencher (CR2411131, Servicebio, China) was added, and the fluorescence signal of the cells was detected using confocal microscopy.

Tissue immunofluorescence staining and immunohistochemical staining

Mouse tissue samples were fixed in 4% paraformaldehyde (PFA) at room temperature and embedded in paraffin. Sections of 5 μm thickness were obtained by paraffin sectioning of mouse tissues using a paraffin slicer. After dewaxing and hydration, mouse tissues were stained for PPAR-α, PPAR-γ, H3K9ac, p-NF-κB, SIRT1, SIRT4, P16, and other proteins according to the incubation procedures described above for the primary and fluorescent secondary antibodies in the cellular immunofluorescence assay. PI3K and Glut1 proteins were incubated with HRP-labelled secondary antibodies for immunohistochemical staining. After completion of tissue immunofluorescence and immunohistochemical staining, the slices were sealed with neutral resin and imaged using a tissue scanner (Science, Winmedic Tech. Co., Ltd., China) and a fluorescent tissue scanner (Pannoramic MIDI, 3DHISTECH, Hungary).

Bioinformatics Analysis

The visualization results of the bioinformatics analysis presented in this study were obtained using the bioinformatics cloud platform of Shanghai Oebiotech Co., Ltd. The raw transcriptomic, proteomic, and acetylation-modified proteomic data of red light-treated keratinocytes were imported into the KEGG analysis, Volcano Diagram, and Chord Diagram templates of differentially expressed genes and differentially expressed proteins of the Oebiotech Cloud Platform, according to the format required by the platform, to obtain the visualized analysis results.

Gene silencing of SIRT4

10^5 PAM212 cells were seeded into 12-well plates (medium volume of 900 μL per well) and allowed to attach to the wall overnight. When cell fusion reached 30%-50%, the fresh medium containing the transfection reagent was replaced (810 μL complete medium + 90 μL transfection reagent). The transfection reagent was divided into solutions A and B. Solution A contained 25 pmol si-SIRT4 (50 μM, 5 μL), 50 μL Opti-MEM™ I Reduced Serum Medium (31985062, Thermo Fisher, China), and solution B contained 50 μL Opti-MEM, 3 μL Lipofectamine RNAiMAX Transfection Reagent (13778075, Thermo Fisher, China). The transfection complex was prepared by adding solution A to solution B, mixing well, and incubating for 5-10 min at room temperature. PAM212 cells cultured with the transfection complex were incubated at 37 °C in a 5% CO2 atmosphere for 96 h. Samples were collected at 48 h to detect the level of SIRT4 gene silencing (Qpcr) and at 96 h to detect the level of SIRT4 protein (Western blot, cellular immunofluorescence).

PET/CT in vivo metabolic assay

Metabolic levels were measured using PET/CT in mice (2Y+R) 2 years after periodic red light treatment. A metabolically active positive control group of 4-month-old (4M) mice was used. The control group consisted of 2-year-old mice (2Y) without periodic red light treatment. After overnight fasting, the mice in the 4M, 2Y, and 2Y+R groups were weighed and injected with the corresponding dose of the radiotracer ^{18}F-FDG at a dose of 4 MBq/kg. After the tracer entered the blood circulation, the mice were secured on the contrast bed with adhesive tape and visualized using a PET-CT meter to develop images. The effects of cyclic red light irradiation on the metabolism of mice were determined by analyzing the amount of radioactivity in the 4M, 2Y, and 2Y+R groups using PET-CT.

Cellular reactive oxygen species assay (DCFH/Mito-sox)

For intracellular ROS detection, we used DCFH-DA and Mito-SOX probes to detect cytoplasmic reactive oxygen species and mitochondrial reactive oxygen species in cells, respectively. For cytoplasmic ROS detection, PAM212 cells were incubated with 10 μM DCFH-DA probe for 0.5 h at 37 °C after red light irradiation. Fluorescence imaging was performed using a fluorescence microscope (CKX53SF, Olympus, Japan). The fluorescence intensity of the DCFH-DA probe in the cells was measured using a multimode microplate reader (SpectraMax M5, Molecular Devices, USA). For mitochondrial ROS detection, cells were incubated with 5 μM Mito-SOX for 15 min, and the fluorescence intensity of the Mito-SOX fluorescent probe in the cells was characterized using a fluorescence confocal microscope and a Multi-Mode Microplate Reader.

DHE tissue reactive oxygen species assay

After snap-freezing the dorsal skin tissues of the mice in liquid nitrogen, Service Biotechnology Co., Ltd. prepared frozen sections of the skin tissues, performed ROS fluorescence staining (using Dihydroethidium, DHE), and conducted imaging analysis using a fluorescent tissue scanner.

H&E staining

Normal and scarred skin of mice were treated with 4% PFA and embedded in paraffin. The treated skin sample slices (5 μm) were subjected to H&E staining after deparaffinization and rehydration. Imaging was performed using a tissue slice scanner (Science, Winmedic Tech, China).

Statistics and reproducibility

The blots presented in this study were performed in at least three replicates, and a minimum of three fields of fluorescence images were collected for fluorescence experiments. GraphPad Prism 9 software was used for statistical analysis, and the number of repetitions for all experimental settings was ≥3. Experimental animal grouping was performed using random assignments. Data are presented as the mean ± SD. Student's *t*-test or one-way ANOVA was performed to determine statistical significance. Statistical significance was set at $P < 0.05$ (*$P < 0.05$; **$P < 0.01$; ***$P < 0.001$; ****$P < 0.0001$).

Result

1. Periodic red light irradiation recovers histone acetylation and metabolism in the skin of naturally aging mice

The aging phenotype of the skin is jointly regulated by genetic and epigenetic factors[46]. However, the relationship between red light-driven metabolic regulation, histone acetylation, and skin aging has not yet been elucidated. We observed that red light irradiation at doses ranging from 0 to 160 J/cm² enhanced keratinocyte activity, with a 20% increase in cellular activity at 80 J/cm² (Fig 1a). Simultaneously, within the 0–160 J/cm² range, the acetylation levels of histone H3, particularly H3K9ac, exhibited a progressive increase as the red light irradiation dose escalated (Fig 1b and S1a). Following treatment with 80 J/cm² red light irradiation, we observed reduced β-galactosidase activity in H_2O_2-induced oxidative senescence keratinocytes (Fig 1c), alongside decreased expression of the cell cycle arrest proteins P16 and P21. In contrast, nuclear Lamin B1 (LAMB1), which is associated with cell proliferation, showed increased expression (Fig S1b). The enrichment levels of H3K9ac in the promoter regions of the anti-ageing related genes *SOD2*, peroxisome proliferator-activated receptor gamma coactivator 1-alpha (*Ppargc1α*), and *LAMB1* were significantly increased (Fig 1d-h). Furthermore, the expression of senescence-associated SASP inflammatory factors also exhibited a marked downward trend (Fig S1c). These findings preliminarily demonstrate that a specific dose of red light promotes histone acetylation at the H3K9 site. As a key histone acetylation site regulating cellular inflammation and senescence, this may explain how red light alleviates oxidative senescence in keratinocytes.

To further investigate the effects of red light on skin tissue aging in vivo, we established a mouse model of natural aging under conditions of periodic red light irradiation (Fig S1d and e). As shown in Fig S1e, 2-year-old mice exhibited pronounced facial aging characteristics compared to 4-month-old mice, including significant whisker loss and age-related ocular pathology (Fig 1e). During the treatment protocol for our naturally aging mouse model, 1-and 2-year-old mice underwent three and nine 15-day red light irradiation treatments, respectively (Fig S1d). To preclude potential neuromodulatory effects, we employed restraints and light-blocking fabric during red light exposure to restrict the movement of the mice and prevent direct illumination of the eyes (Fig S1f). Prior to and following red light irradiation, we employed infrared detectors to monitor changes in the surface body temperatures of the mice. The results indicated that after exposure to 80 J/cm² of red light, the temperature of the mice increased from 35.9°C to 36.1°C (Fig S1g). This demonstrates that our irradiation protocol did not induce a significant thermos effect. Subsequent analysis of skin and tissue samples from the animal model revealed that periodic red light irradiation did not induce pathological changes in any organ or tissue, including the brain, heart, liver, spleen, lungs, kidneys, or skin (Fig S1g). Indeed, beneficial alterations in aging characteristics were observed across multiple organs and tissues, such as a marked reduction in monocyte numbers within the cardiac muscle tissue (Fig S1i-o). A marked decline in H3K9ac levels was observed in the stratum corneum with advancing age (Fig 1i). In contrast, following periodic red light treatment, H3K9ac levels were increased in the stratum corneum of both 1-year-old and 2-year-old mice (Fig 1j), along with a marked elevation in total H3K9ac within aged skin tissue (Fig 1k). Furthermore, we quantified the relative fluorescence intensity of the P16 protein and the proportion of LAMB1-positive cells in the aged skin tissue. We found that periodic red light

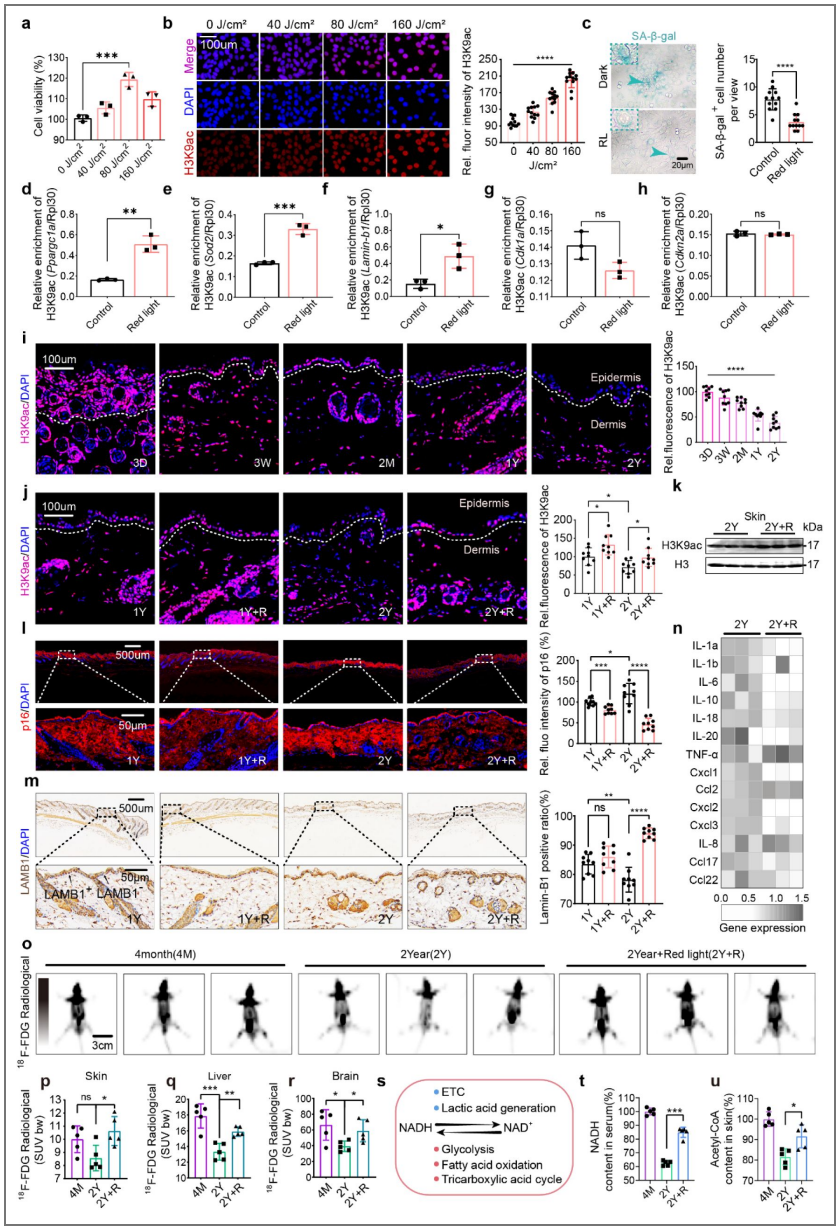

Figure 1. Periodic red light irradiation treatment leads to increased H3K9ac and metabolism in skin tissues of a senescent mouse model.

a, CCK-8 analysis of keratinocyte activity after red light treatment, n=3. **b,** Fluorescence images of H3K9ac protein in keratinocytes after treatment with different doses of red light. **c,** Image of β-galactosidase staining in senescent keratinocyte model after red light irradiation treatment. **d-h,** ChIP-qPCR experiments were conducted to assess the enrichment of H3K9ac in the promoter regions of *Ppargc1a* (**d**), *Sod2* (**e**), *Lamin-b1* (**f**), *Cdkn1a* (**g**) and *Cdkn2a* (**h**). Following ChIP experiments using the H3K9ac antibody or control IgG, qPCR analysis was performed using primers targeting the promoters of these genes, RPL30 is used as an internal standard for the calibration of the target gene, n=3. **i,** Fluorescence images of H3K9ac (red) protein in skin tissues of mice of different ages (DAPI, blue), histogram shows the relative quantification of the red signal within the white dashed line in **i,** n=9. **j,** Fluorescence images of H3K9ac (red) proteins in skin tissues of one- and two-year old mice after red light irradiation treatment (DAPI, blue). histogram shows the relative quantification of the red signal within the white dashed line in **j,** n=9. **k,** The evels of H3K9ac and H3 proteins in the skin of mice in groups 2Y and 2Y+R, n=3. **l** and **m,** The levels of P16(**l**) and LAMB1(**m**) proteins in the skin of mice in groups 4M, 2Y and 2Y+R. **n**, The expression heatmap of SASP inflammatory factors in the skin of mice in groups 2Y, and 2Y+R, n=3. **o, p, q** and **r,** PET/CT images (**o**) and ^{18}F-FDG Radiological signals in skin (**p**), liver (**q**) and brain (**r**) of mice in the 4M, 2Y and 2Y+R treatment groups, n=6. **s,** The conversion process of NAD^+ and NADH in keratinocytes. **t,** Relative levels of NADH in serum of mice in the 4M, 2Y and 2Y+R groups, n=5. **u,** Relative content of Acetyl-CoA in the skin tissues of mice in groups 4M, 2Y and 2Y+R, n=5.

treatment not only reduced P16 protein expression and increased the proportion of LAMB1-positive cells (Fig 1l and m) but also decreased the expression levels of SASP inflammatory factors in the skin tissue (Fig 1n). This shift in the expression patterns of aging markers and age-related inflammatory factors suggests the anti-aging effects of periodic red light irradiation on the skin.

Another prominent feature of aged tissues is a decline in cellular metabolism. Therefore, we further examined the metabolism of ^{18}F-FDG in the skin tissues of aged mice using PET-CT. By capturing radioactive signals, we found that periodic red light irradiation not only increased the radioactive signal in the cortex of aged mice (Fig 1o and p) but also markedly elevated uptake in other organs, such as the liver and brain (Fig 1p, q, and r). This indicates that red light promotes systemic metabolism in aged mice, a finding further supported by increased NADH levels in the peripheral blood (Fig 1s and **t)**. Moreover, red light irradiation elevated the acetyl-CoA levels in the skin tissues of aged mice (Fig 1u). As a key intracellular metabolite, acetyl-CoA serves as the sole substrate for histone acetylation and reflects cellular and tissue metabolic activity. These findings suggest that periodic red light treatment may enhance metabolic processes, such as glycolysis, fatty acid metabolism, and the TCA cycle, thereby promoting histone acetylation.

2. Red light irradiation increases the metabolic flux and cellular acetyl-CoA content in keratinocytes

To identify the metabolic remodeling effects of red light, building upon the promotion of keratinocyte activity observed at 80 J/cm² (Fig 1a), we further examined the effects of red light on cell migration and proliferation. Scratch assay results demonstrated that the wound closure rate in keratinocytes increased from 40% to 60% 24 h after red light treatment (Fig 2a). Moreover, within 24 h of red light irradiation, the keratinocyte proliferation rates were markedly higher than those in the control group (Fig 2b). Since cellular metabolic levels are closely linked to proliferation, viability, and migration, we further assessed keratinocyte uptake of two major metabolic substrates—glucose and fatty acids—from the culture medium within 12 h of red light treatment. As demonstrated in Fig 2c and Fig 2d, after 12 h of red light treatment, the uptake of both glucose and fatty acids from the medium increased by approximately 10% compared to that in the control group. Under this conditions, the mitochondrial membrane potential was significantly increased (Fig 2e). These findings indicate that red light irradiation enhances the metabolic flux in keratinocytes and boosts mitochondrial metabolic function.

Interestingly, upon further examination of key metabolites associated with intracellular redox status and glycolytic pathways across a red light dose gradient of 0–160 J/cm^2, we observed a pronounced biphasic dose response in ATP levels and the two primary reducing agents, GSH and NADPH (Fig 2f, g, and h). The concentrations of ATP, GSH, and NADPH increased with red light irradiation dose within the 0–80 J/cm² range, revealing a potential reason for keratinocyte activity peaking at 80 J/cm² red light conditions and indicating that red light promotes cellular metabolism (Fig 1a and Fig 2f-h). Moreover, our assessment of the mitochondrial membrane potential and cellular reactive oxygen species (ROS) in keratinocytes under varying red light doses revealed that mitochondrial ROS production increased with increasing red light exposure (Fig 2i). Interestingly, the overall level of reactive oxygen species within keratinocytes exhibited a decreasing trend across the red light dose range of 0–80 J/cm² (Fig 2j). Considering that cytoplasmic GSH and NADPH levels also increased with increasing red light doses within the 0–80 J/cm² range (Fig 2g and h), we propose that the biphasic dose effect driven by red light is most likely mediated through the neutralization of mitochondrial ROS by cellular reducing agents. Excessively high red light doses induce excessive mitochondrial ROS production, impair normal cellular processes, and consequently elicit adverse reactions. This is further supported by the observation that the mitochondrial membrane potential levels in keratinocytes begin to decline from their peak at 160 J/cm² red light exposure (Fig S2a).

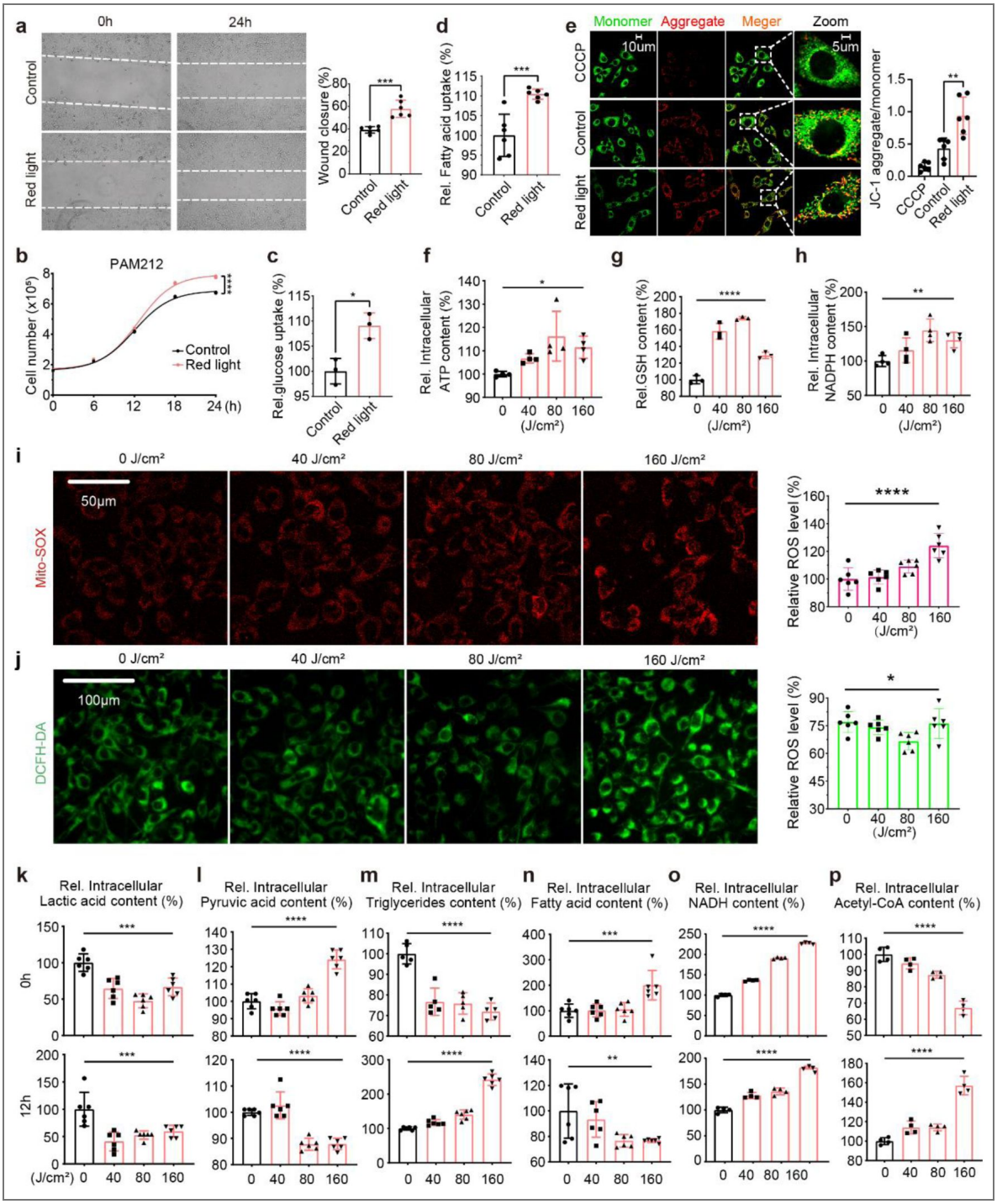

Figure 2. Red light irradiation promotes keratinocyte metabolic reprogramming.

a, Migration of keratinocytes after 24 h of red light treatment (n = 6). **b,** Proliferation of keratinocytes: 0–24 h after red light treatment (n = 3). **c** and **d,** Uptake of glucose (**c**, n=3) and fatty acid (**d**, n=6) in the culture medium by keratinocytes 24 h after red light treatment. **e,** Mitochondrial membrane potential of keratinocytes after red-light treatment. CCCP, Carbonyl cyanide m-chlorophenylhydrazone (n=6). **f,** Graded-dose red light treatment affects ATP production in keratinocytes (n = 4). **g** and **h,** Relative changes in cellular GSH (**g**) and NADPH (**h**) contents 12 h after treatment of keratinocytes with graded doses of red light (n=3). **g** and **h,** Fluorescence images of total reactive oxygen species (ROS) levels (**i**, n=6) and mitochondrial ROS levels (**j**, n=6) in keratinocytes under different red light doses. **k-p,** Relative changes in intracellular lactate (**k**, n=6), pyruvate (**l**, n=6), triglyceride (**m**, n=6), fatty acid (**n**, n=6), NADH (**o**, n=4), and acetyl-CoA (**p**, n=4) at 0h and 12h after treatment of keratinocytes with graded doses of red light.

Regarding changes in metabolite levels following red light irradiation, we compared intracellular lactate, pyruvate, triglyceride, and fatty acid concentrations at 0 and 12 h post-red light exposure (Fig 2k-n). We observed that, apart from lactate exhibiting a sustained decline within 12 h post-red light, the other three metabolites demonstrated distinct temporal patterns of change within 12 h of red light treatment (Fig 2k-n), with increased cellular utilization of fatty acids (Fig 2m and n). These findings suggest that the metabolic effects of red light involve accelerated aerobic metabolism and fatty acid oxidation. Based on the conversion relationships between the aforementioned metabolic pathways, as depicted in Fig 1s, we reassessed the NADH levels in keratinocytes at 0 and 12 h after red light treatment. The results revealed an increasing trend in NADH content at both time points (Fig 2o). These findings conclusively demonstrate that red light irradiation promotes cellular metabolic processes, including glycolysis, fatty acid metabolism, and the TCA cycle. This aligns with the observations in animal aging models. Finally, we measured the acetyl-CoA levels in keratinocytes following red light irradiation. Although red light rapidly depleted acetyl-CoA, both acetyl-CoA content and H3K9ac levels increased with increasing red light dose at 12 h post-treatment (Fig 2p and 1b). The concentration of acetyl-CoA in the cell nucleus also increased following exposure to red light (Fig S2b). These results further demonstrates the potential of red light to influence cellular aging by driving histone acetylation through metabolic regulation.

3. Red light modulates cellular metabolism by activating the PI3K-AKT metabolic pathway and PPAR-α

Red light accelerates mitochondrial metabolism by enhancing cellular metabolic flux, thereby promoting the accumulation of acetyl-CoA in keratinocytes and aged skin tissue. This mechanism may explain how red light facilitates histone acetylation and mitigates aging (Fig 3a). To adress the precise regulatory mechanism of red light on cellular glycolipid metabolism, we conducted a transcriptomic analysis of keratinocytes following red-light treatment. KEGG pathway enrichment analysis of the transcripts revealed that the top 20 significantly altered pathways included multiple signalling pathways related to cellular metabolism and aging, such as the p53/PPAR/PI3K-AKT/MAPK signalling pathway (Fig 3b). Furthermore, genes showing significant changes exhibited an overall trend of increased expression levels (Fig 3c), suggesting that red light enhances the transcriptional output across the genome. Given our observation that numerous photobiological regulatory effects of red light correlate with cellular metabolism, we focused on metabolically relevant signalling pathways enriched in transcripts. Consequently, the enrichment of the glucose metabolism pathway (PI3K-AKT signalling pathway) and the fatty acid metabolism regulation pathway (PPAR signalling pathway) in transcripts drew our attention (Fig 3b). Notably, upon further analysis of the metabolic pathways and metabolism-related genes upregulated in transcripts, we observed the upregulation of key genes in the PPAR/PI3K-AKT signalling pathway, including the fatty acid transporter gene *Cpt1a*, the key FAO transcription factor *PPAR-α*, and multiple PI3K family genes (Fig 3d). Through a precise analysis of fold-change variations in metabolic gene expression, we identified markedly elevated expression levels of genes involved in glycolysis, the TCA cycle, the pentose phosphate pathway, and fatty acid oxidation (Fig 3e). Fatty acid metabolism and glycolysis/gluconeogenesis pathways were enriched, with the upregulation of fatty acid metabolism being the most pronounced across all pathways (Fig 3f). These findings suggest that red light may activate cellular glycolytic and lipid metabolism by separately stimulating the aforementioned signalling pathways, thereby mobilizing overall cellular metabolic vigor.

Similarly, proteomic analysis of keratinocytes following red light treatment revealed that both dark and red light conditions significantly influenced protein expression patterns within keratinocytes (Fig 3g). Genome-wide signature analysis (GSEA) of differentially expressed proteins further enriched the gluconeogenesis and PPAR signalling pathways in keratinocytes under dark versus red light conditions (Fig 3h and i). Within the proteomic findings, we further observed elevated levels of proteins belonging to the GPCRs family (Fig S3a and b). As

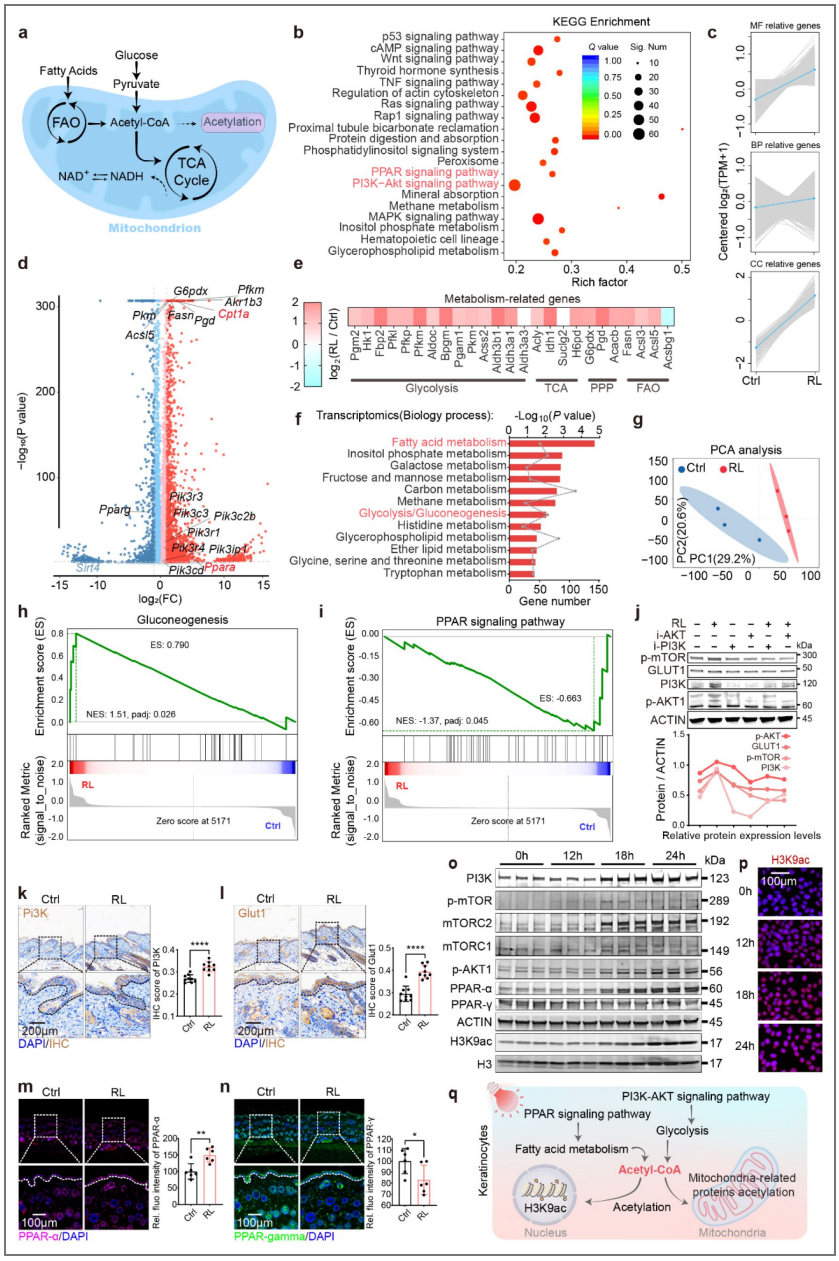

Figure 3. Red light activated the Pi3k-akt signalling pathway and PPAR-α in keratinocytes simultaneously with H3k9ac.

a, Schematic representation of substance metabolism in mitochondria. **b,** Scatterplot of significantly enriched functions for transcript data from keratinocytes treated with red light (Top 20 KEGG for plotting). **c,** Differential gene module expression trend line graph. Coloured lines indicate the mean value of the change for this group of genes. **d,** Volcano plot of the differences in gene expression after red light treatment. **e,** Expression of keratinocyte metabolism-related genes after red light treatment. **f,** Enrichment analysis of metabolic pathways after red light treatment (*P* value > 0.5). **g,** Principal component analysis (PCA) of keratinocyte proteomics in the red light and dark treatment groups, n=3. **h** and **i,** GSEA analysis of gluconeogenesis (**h**) and PPAR signalling pathway (**i**) proteins in keratinocytes after red light irradiation. **j,** Expression levels of p-mTOR, Glut1, Pi3k, and p-AKT proteins in keratinocytes after red light treatment in the presence of AKT and PI3K inhibitors (n = 3). **k** and **l,** Immunohistochemical staining of PI3K (**k**) and Glut1(**l**) proteins in skin tissues after red light irradiation, n=9. **m** and **n,** Immunofluorescence staining of PPAR-α and PPAR-γ proteins in skin tissues after red light irradiation (n = 9). **o,** Changes in the levels of PI3K, p-mTOR, Raptor, Rictor, p-Akt, PPAR-α, PPAR-γ, p-S6, H3K9ac, and H3 proteins in keratinocytes at 0h, 12h, 18h, and 24h after red light treatment, n=3. **p,** Fluorescence images of H3K9ac protein at different time points after red light treatment in keratinocytes. **q,** Schematic diagram of increased glycolipid metabolism driving histone acetylation in cells after red light treatment of keratinocytes. Ctrl: Control; RL: Red light.

upstream regulators of the PI3K-AKT signalling pathway, the enrichment of molecular processes involving GPCRs in the proteomic analysis of keratinocytes following red light exposure indirectly indicates the regulatory role of red light in the PI3K-AKT pathway.

In summary, these findings suggest that red light treatment activates intracellular glycolytic and lipid metabolic pathways. Consequently, we validated these two signalling pathways at both the cellular and tissue levels. First, we examined the effects of red light on glycolytic pathways. Given that cellular glycolysis is primarily regulated through the coordinated action of the metabolic control centre mTOR and the PI3K-AKT signalling pathway, we initially assessed changes in key protein levels within these pathways at the cellular level. We observed a marked increase in protein levels along the mTOR/PI3K-AKT/Glut1 signalling axis following red light treatment (Fig 3j). Inhibition of this axis was achieved by administering either a PI3K inhibitor or an AKT inhibitor. Crucially, red light treatment under inhibitor conditions partially mitigated this suppression, confirming the role of red light in promoting protein expression along this axis at the cellular level. At the tissue level, we validated the expression of PI3K and Glut1 in the skin tissue following red light treatment. Immunohistochemical staining results also revealed increased PI3K and Glut1 signalling (Fig 3k and l).

Furthermore, we independently validated alterations in PPAR-α and PPAR-γ levels, which are key regulators of lipid metabolism and synthesis, at both cellular and tissue scales. After red light treatment, cellular and tissue PPAR-α levels increased, whereas PPAR-γ levels decreased (Fig 3m and n). To characterize the regulation of H3K9ac by red light-activated glycolipid metabolism, we examined the temporal dynamics of glycolipid metabolism activation and H3K9ac changes in keratinocytes within 24 h of red light exposure. Surprisingly, the results indicated that key proteins within the PPAR-α/PI3K-AKT signalling pathway began to significantly increase 12 h after red light cessation, occurring almost simultaneously with the increase in H3K9ac levels (Fig 3o). Fluorescence imaging of H3K9ac within 24 h of red light irradiation similarly demonstrated a progressive elevation in H3K9ac levels (Fig 3p). These findings confirm that red light can independently activate the PI3K-Akt and PPAR-α pathways to regulate cellular glycolipid metabolism at the cellular level. Combined with the experimental findings of increased acetyl-CoA levels in keratinocytes at 12 h post-red light irradiation (Fig 2p), we ultimately elucidated a potential mechanism by which red light promotes acetylation-related processes in keratinocytes by activating glycolipid metabolic pathways, leading to cellular acetyl-CoA accumulation (Fig 3q).

4. Red light mediates histone acetylation primarily via lipid metabolism

We demonstrated that red light activates intracellular glycolipid metabolic pathways and histone acetylation. However, the mechanism by which mitochondrial metabolism is activated under red light conditions and the relationship between metabolic pathway activation and histone acetylation remain unclear. We need to further clarify whether histone acetylation driven by metabolic activation in keratinocytes under red light irradiation exhibits metabolic specificity and how red light directly influences mitochondrial metabolic processes.

To investigate the direct effects of metabolism on histone acetylation, we first treated keratinocytes with agonists and inhibitors of the key glycolytic and lipolytic proteins AKT1 and PPAR-α, respectively. Subsequently, we examined the impact of histone acetylation on glycolytic and lipolytic pathways under red light conditions by inhibiting acetyltransferases and deacetylases. Finally, we used inhibitors of glucose and lipid metabolism to establish the regulatory role of red light-induced metabolic activation of H3K9ac under red light exposure. The results revealed that the AKT agonist SC-79 significantly promoted H3K9ac levels (Fig 4a and b). However, while the AKT inhibitor MK2206 markedly suppressed p-mTOR levels, it did not significantly inhibit histone acetylation (Fig 4c and d). Conversely, intracellular acetyl-CoA levels were markedly increased and decreased by SC-79 and MK2206, respectively (Fig 4e and f). Similarly, we performed experiments with the PPAR-α agonist, WY14643, and the PPAR-α antagonist, GW6471. We found that activating PPAR-α markedly promoted H3K9ac, but had no

significant effect on p-mTOR or p-AKT levels (Fig 4g and h). Inhibition of PPAR-α similarly reduced histone acetylation (Fig 4i and j). Intracellular acetyl-CoA levels exhibited a pronounced dose-dependent response to both WY14643 and GW6471 (Fig 4k and l). These findings conclusively demonstrate that acetyl-CoA derived from lipid metabolism serves as the primary acetyl donor for red-light-driven H3K9ac.

In subsequent experiments, we inhibited histone acetylation using the histone acetyltransferase inhibitor Nicur (a curcumin-derived p300/CBP inhibitor) and observed that Nicur appeared to exert no discernible effect on the glycolytic pathway. Moreover, following red light treatment, both the intracellular glycolytic pathway and H3K9ac exhibited pronounced activation trends (Fig 4m). Conversely, when histone acetylation was inhibited using the deacetylases inhibitor Trichostatin A (TSA), the levels of proteins associated with the glucose metabolism pathway showed a decreasing trend (Fig 4n). In contrast to glucose metabolism, TSA treatment markedly increased PPAR-α expression, and red light irradiation further amplified this effect (Fig 4n). This regulatory effect was not pronounced under Nicur treatment (Fig 4m). In both sets of experiments, red light treatment increased intracellular H3K9ac levels (Fig 4m, n and Fig S4a, b). These findings further validate that red light-induced metabolic activation directly causes H3K9ac increase rather than indirectly through regulation of histone acetyltransferases and histone deacetylases. These results indicate that histone acetylation preferentially promotes the expression of lipid metabolism-related proteins. Further treatment of keratinocytes with the glucose metabolism inhibitor MK2206 revealed that red light still upregulated H3K9ac, whereas treatment with the lipid metabolism inhibitor GW6471 abolished the ability of red light to increase intracellular H3K9ac levels. This demonstrates that red light-driven lipid metabolism plays a fundamental role in elevating H3K9ac levels (Fig 4o and p).

Existing research indicates that cytochrome c oxidase is the direct target of red light within mitochondria[50]. We propose that the transient effect of red light on cellular metabolic regulation (changes in intracellular metabolite levels at 0 h after red light exposure) is also linked to the response of cytochrome c oxidase to red light within the mitochondria (Fig 2k-p). Consequently, we independently inhibited the electron transport chain and cytochrome c oxidase in keratinocytes treated with red light. The results revealed that disruption of the electron transport chain abolished the regulatory capacity of red light over metabolic pathways and histone acetylation (Fig 4q). Similarly, under cytochrome c oxidase inhibition, red light treatment failed to increase histone acetylation and consequently lost its regulatory effect on the glycolipid metabolic pathway (Fig 4r). Furthermore, following cytochrome c oxidase inhibition, the pattern of transient intracellular key metabolite regulation after red light irradiation changed (Fig 4s-v), and the effects of red light on lactate and acetyl-CoA content were reversed (Fig 2k, p and Fig 4s, v). Additionally, cellular component enrichment analysis of the acetylated proteomics data also revealed that multiple mitochondrial processes were significantly upregulated following red light treatment (Fig S4c and d). Collectively, these findings demonstrate that the transient metabolic drive induced by red light is mediated by cytochrome oxidase within the mitochondria.

Based on these experimental findings, we elucidated the mechanism by which red-light irradiation modulates intracellular H3K9ac levels. Specifically, red light first drives mitochondrial metabolism in keratinocytes via cytochrome c oxidase, altering metabolite concentrations and activating relevant signalling pathways. This ultimately manifests the characteristic biological regulatory effect of red light: it activates intracellular glycolipid metabolism and primarily promotes histone acetylation within keratinocytes via acetyl-CoA supplied by fatty acid metabolism.

5. Downregulation of SIRT4 induced by red light alleviates oxidative ageing in keratinocytes

Although red light exerts transient regulatory effects by directly driving mitochondrial metabolism, the mechanisms and molecular targets by which it subsequently activates lipid metabolism and mediates H3K9ac remain unclear.

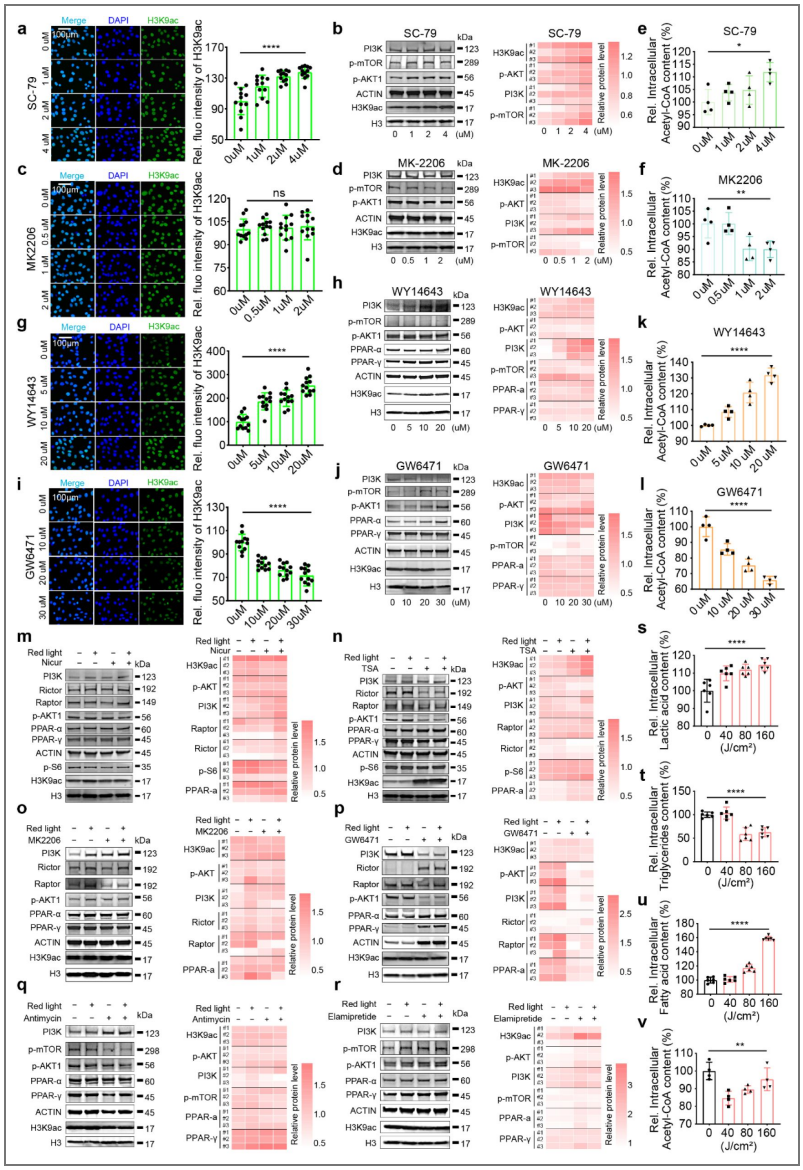

Figure 4. Red light drives metabolism through mitochondria and mediates histone-acetylation primarily through lipid metabolism.

a and **b,** Fluorescence images of H3K9ac (green, **a**, n=12) protein and levels of PI3K, p-mTOR, p-AKT, H3K9ac and H3 proteins (**b**, n=3) in keratinocytes under different concentrations of SC-79 treatment conditions (DAPI, blue). **c** and **d,** Fluorescence images of H3K9ac (green, **c**, n=12) protein and levels of PI3K, p-mTOR, p-AKT, H3K9ac and H3 proteins (**d**, n=3) in keratinocytes under different concentrations of MK2206 treatment conditions (DAPI, blue). **e** and **f,** Effects of different concentrations of SC-79 **(e)** and MK2206 **(f)** on Acetyl-CoA content in keratinocytes, n=4. **g** and **h,** Fluorescence images of H3K9ac (green, **g**, n=12) protein and levels of PI3K, p-mTOR, p-AKT, PPAR-α, PPAR-γ, H3K9ac and H3 proteins (**h**, n=3) in keratinocytes under different concentrations of WY14643 treatment conditions (DAPI, blue). **i** and **j,** Fluorescence images of H3K9ac (green, **i**, n=12) protein and levels of PI3K, p-mTOR, p-AKT, PPAR-α, PPAR-γ, H3K9ac and H3 proteins (**j**, n=3) in keratinocytes under different concentrations of GW6471 treatment conditions (DAPI, blue). **k** and **l,** Effects of different concentrations of WY14643 **(k)** and GW6471 **(l)** on Acetyl-CoA content in keratinocytes, n=4. **m** and **n,** Effect of red light treatment on the levels of PI3K, p-mTOR, Raptor, Rictor, p-AKT, PPAR-α, PPAR-γ, p-S6, H3K9ac and H3 proteins in keratinocytes in the presence of 5uM Nicur **(m)** and TSA **(n)**, n=3. **o** and **p,** Effect of red light treatment on the levels of Pi3k, Raptor, Rictor, PPAR-α, PPAR-γ, p-S6, H3K9ac and H3 proteins in keratinocytes in the presence of 2uM Mk2206 **(o)** and 20uM GW6471 **(p)**, n=3. **q** and **r,** Effect of red light treatment on the levels of PI3K, p-mTOR, p-AKT, PPAR-α, PPAR-γ, H3K9ac and H3 proteins in keratinocytes in the presence of 5uM Antimycin **(q)** and Elamipretide **(r)**, n=3. **s, t, u,** and **v,** Relative contents of lactate (**s**, n=6), triglycerides (**t**, n=6), fatty acids (**u**, n=6) and Acetyl-CoA (**v**, n=4) in keratinocytes after irradiation of 5uM Elamipretide-treated keratinocytes with graded doses of red light.

Among the changes in keratinocyte total protein expression, the significant reduction in SIRT4 protein levels following red light treatment drew our attention (Fig 5a and b). As a member of the Sirtuin protein family, SIRT4 possesses deacetylase activity. The reduction in SIRT4 levels leads to increased protein acetylation, consistent with our experimental findings. Furthermore, as a deacetylase primarily distributed in the mitochondria, SIRT4 has been reported to regulate cellular metabolism, particularly fatty acid oxidation processes, by modulating the acetylation of mitochondrial metabolism-related proteins (Fig 5c). Moreover, SIRT4 modulates PPAR-α activation by inhibiting SIRT1 activity, thereby regulating NF-κB-mediated inflammatory signalling[51]. This aligns with our observation that red light irradiation alleviates inflammatory factor expression in oxidatively aged keratinocytes and tissues, as well as in naturally aged skin (Fig S1c and Fig 1n). Therefore, we propose that the reduction in SIRT4 protein levels following red light irradiation may be the primary mechanism underlying the enhanced mitochondrial metabolism observed after red light treatment.

To further validate the proteomics analysis results and our hypothesis, we first verified SIRT4 expression in keratinocytes exposed to red light. We found that SIRT4 levels progressively decreased with increasing light doses (Fig 5d and f), whereas SIRT1 levels increased (Fig 5e and f). Moreover, under red light treatment, the trend in SIRT4 levels mirrored that of p-NF-κB, while exhibiting the opposite pattern to that of PPAR-α (Fig 5g). These findings validate the regulatory capacity of SIRT4 on intracellular lipid metabolism targets and inflammatory signalling pathways. We also assessed SIRT1/4 protein expression levels in aged animal models. Similarly, we observed a progressive increase in SIRT4 expression in tissues with advancing age, whereas SIRT1 expression exhibited an inverse trend (Fig 5h and i). Red light treatment significantly downregulated Sirt4 protein expression in aged skin tissue (Fig 5h and i). Moreover, age-related p-NF-κB activation in the skin tissue was markedly suppressed following periodic red light exposure (Fig 5j, k and Fig S5a). At both the cellular and tissue levels, we observed a negative correlation between PPAR-α and p-NF-κB protein expression levels (Fig S5b, c). This negative correlation was more pronounced in keratinocytes under red light (Fig S5b). These findings suggest that reduced SIRT4 protein content plays a substantial role in the red light-driven cellular anti-aging effects.

Therefore, to further elucidate the role of SIRT4 in cellular senescence, we employed siRNA to silence SIRT4 expression in keratinocytes. Following a marked reduction in both transcriptional and protein expression levels of SIRT4 within the keratinocytes (Fig 5l and m), we observed a significant increase in cellular activity, along with elevated intracellular acetyl-CoA levels (Fig 5n and o). These findings demonstrate that SIRT4 downregulation promotes cellular metabolism. Furthermore, we observed a marked increase in PPAR-α protein levels, activation at histone H3K9 sites, reduced expression of senescence factors p16 and p21, and elevated Lamin-B1 in Sirt4-silenced cells (Fig 5p-s). Nf-κB phosphorylation levels and SASP-associated inflammatory cytokine secretion were also reduced in the si-SIRT4-treated group (Fig 5r and t). Furthermore, by measuring galactosidase activity in keratinocytes following si-SIRT4 treatment, we found that SIRT4 downregulation significantly alleviated senescence in the keratinocyte oxidative ageing model (Fig 5u). These findings conclusively demonstrate the positive role of SIRT4 in keratinocyte anti-aging processes, revealing that red light-driven downregulation of SIRT4 protein levels may constitute a key mechanism underlying these effects.

6. Red light activates fatty acid oxidation by inhibiting the SIRT4-MCD axis

Given that SIRT4 is a mitochondrial-localised deacetylase, current research suggests that SIRT4 participates in the regulation of mitochondrial fatty acid oxidation by deacetylating malonyl-CoA decarboxylase (MCD)[52]. This is consistent with our observation that red light mediates H3K9ac via lipid metabolism. Therefore, in order to further investigate and elucidate the mechanisms underlying the anti-ageing effects of red light, we conducted acetylation proteomic analysis of keratinocytes following red light treatment.

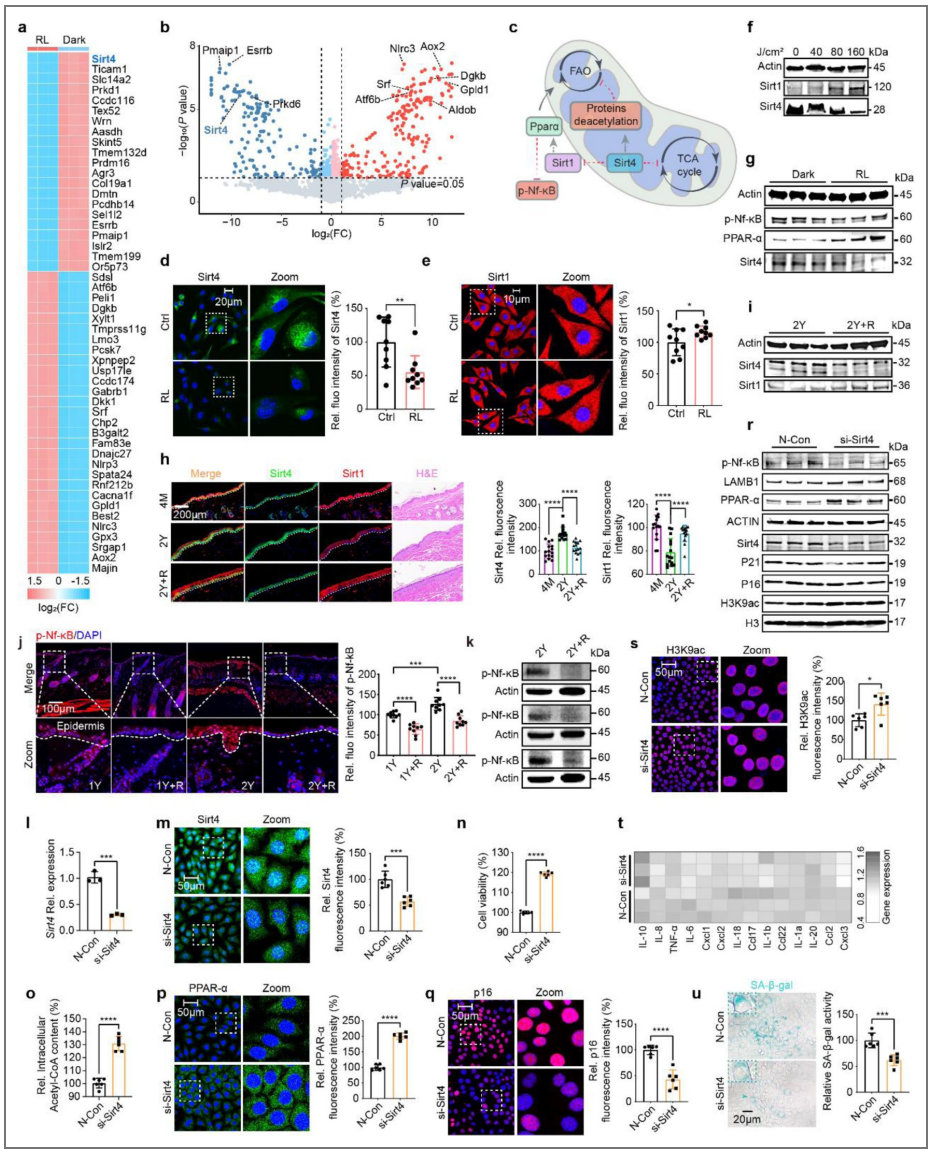

Figure 5. Red light-induced downregulation of SIRT4 is primarily responsible for the activation of lipid metabolism, alleviation of inflammation, and resistance to aging in keratinocytes.

a, Heatmap showing the top 50 significantly differentially expressed proteins in red light-irradiated keratinocytes. **b,** Volcano plot of protein content changes in keratinocytes after red light treatment. **c,** Schematic representation of the role of SIRT4 in mitochondria and cell. **d** and **e,** Fluorescence images of Sirt4 (**d**) and SIRT1 (**e**) protein and nucleus in keratinocytes after red light treatment, n=9. **f,** Intracellular protein levels of SIRT1 and SIRT4 after dose-gradient red light treatment of keratinocytes, n=3. **g,** Protein levels of p-Nf-κB, PPAR-α and Sirt4 in keratinocytes after red light treatment, n=3. **h,** H&E staining images and fluorescence images of SIRT4 (green) and SIRT1 (red) proteins of mouse skin tissues in 4M, 2Y and 2Y+R treatment groups (DAPI, blue), n=3. **i,** The levels of SIRT4 and SIRT1 proteins in the skin of aged mice after cyclic red light treatment, n=3. **j** and **k,** Fluorescence images of p-Nf-κB (red, **j**) in mice skin tissues after red light treatment of 1Y and 2Y senescent mice (DAPI, blue) and the levels of p-Nf-κB protein (**k**) in skin tissues of 2Y senescent mice after red light treatment, n=3. **l** and **m,** Relative expression of SIRT4 mRNA (**l**, n=3) and fluorescence images of SIRT4 protein (green) (**m**, n=6) in keratinocytes after silencing of the SIRT4 gene in keratinocytes using siRNA. **n** and **o,** Changes in cellular activity (**n**, n=3), relative content of intracellular acetyl-CoA (**o**, n=6) in keratinocytes after silencing the SIRT4 gene in keratinocytes using siRNA. **p** and **q,** Fluorescence images of PPAR-α (**p**) and P16 (**q**) proteins in keratinocytes after silencing the Sirt4 gene in keratinocytes using siRNA, n=6. **r,** Protein levels of p-Nf-κB, LAMB1, PPAR-α, Sirt4, p21, p16, H3K9ac, and H3 in keratinocytes after silencing the Sirt4 gene in keratinocytes using siRNA, n=3. **s,** Fluorescence images of H3K9ac proteins in keratinocytes after silencing the SIRT4 gene in keratinocytes using siRNA, n=6. **t,** Relative expression of SASP inflammatory factors in keratinocytes following silencing of the SIRT4 gene in keratinocytes using siRNA, n=3. **u,** Images of β-galactosidase staining in keratinocytes after silencing the SIRT4 gene in keratinocytes cells using siRNA, n=6. N-Con: Negative Control; RL: Red light.

Our analysis revealed increased acetylation levels in numerous metabolism-related proteins after red light irradiation. These proteins are involved in metabolic processes linked to mitochondrial function, such as citrate synthase (CS) and MCD (Fig 6a and b), consistent with the mitochondrial localization and function of SIRT4 (Fig 5c). Furthermore, acetylated proteomics data were significantly enriched in multiple molecular processes involving acetyl-CoA oxidase/dehydrogenase and histone-related processes (Fig 6c and Fig S6a, b), alongside increased acetylation of mitochondrial electron transport chain complex proteins (Fig S6c). Proteins showing increased acetylation following red light irradiation were implicated in biological processes, including fatty acid catabolism, oxidative phosphorylation, the TCA cycle, and pyruvate metabolism (Fig 6d). KEGG pathway analysis of acetylated proteins revealed significant enrichment in fatty acid catabolism and the TCA cycle (Fig 6e). GO analysis identified significantly enriched biological processes, including fatty acid oxidation, histone acetyltransferase activity, and histone deacetylation (Fig S6d and e). Furthermore, combined proteomics and acetylated proteomics analyses revealed that red light-promoted molecular processes were associated with fatty acid oxidation, the TCA cycle, acetyl-CoA transfer, and histone deacetylation processes (Fig 6f). The integration of these multi-omics analyses with existing experimental validation fully elucidates the role of red light in activating intracellular fatty acid oxidation and mitochondrial metabolism.

To further explore the direct link between red light and lipid metabolism, we validated the effects of the SIRT4-MCD axis on cellular fatty acid oxidation and H3K9ac at the keratinocyte level under red light conditions. Within mitochondria, SIRT4 directly inhibits MCD activity through deacetylation, preventing the conversion of malonyl-CoA to acetyl-CoA[52, 53]. The resulting accumulation of malonyl-CoA in the mitochondria strongly inhibited carnitine palmitoyltransferase 1A (CPT1A), a key rate-limiting enzyme in fatty acid oxidation (Fig 6g). In our validation experiments, we observed that in the presence of 5 μM MCD inhibitor CBM-301940, although partial cellular activity was suppressed in keratinocytes, red light irradiation still induced a significant increase in cellular activity. This indicates that the red light-driven increase in cellular activity is not mediated by enhanced lipid metabolism (Fig 6h), but rather by transient effects mediated by photosensitive molecules within the cell, such as cytochrome c oxidase, in response to red light. However, under inhibitor conditions, red light no longer promoted fatty acid uptake by keratinocytes (Fig 6i), and the characteristic red-light-driven increases in ATP and NADH levels in keratinocytes disappeared (Fig 6j and k). Acetyl-CoA content and H3K9ac levels markedly decreased in keratinocytes (Fig 6l, m, and n), and red light irradiation failed to reverse H3K9ac levels (Fig 6m and n). These findings confirm our hypothesis that, following the regulation of keratinocyte metabolism by red light, red light maintains the acetylation of MCD by downregulating SIRT4 levels. This activates MCD function, thereby blocking the inhibitory signals on fatty acid oxidation.

Therefore, when the MCD function is inhibited, red light can no longer achieve PBM, which promotes mitochondrial fatty acid oxidation and the TCA cycle while elevating acetyl-CoA levels in keratinocytes by regulating MCD activity via SIRT4. As acetyl-CoA is the sole acetylation substrate for H3K9ac, this ultimately leads to increased H3K9ac levels in keratinocytes. This mechanism explains the anti-aging effects of red light on the skin observed in our mouse model of natural aging (Fig 1). These findings conclusively demonstrate that the capacity of red light to regulate cellular lipid metabolism and restore acetyl-CoA and H3K9ac levels operates through the SIRT4-MCD axis.

7. Red light alleviated systemic aging in a mouse model of natural aging

Through metabolic characterization and mechanism exploration following red light treatment of cell and animal models, we elucidated the mechanism by which red light activates mitochondrial lipid metabolism and promotes H3K9ac by inhibiting the SIRT4-MCD axis. In mouse models, we validated the tissue penetration depth of red light by measuring its intensity after traversing the mouse skin using photometers, as shown in Fig S7a and b. We found that at a light source height

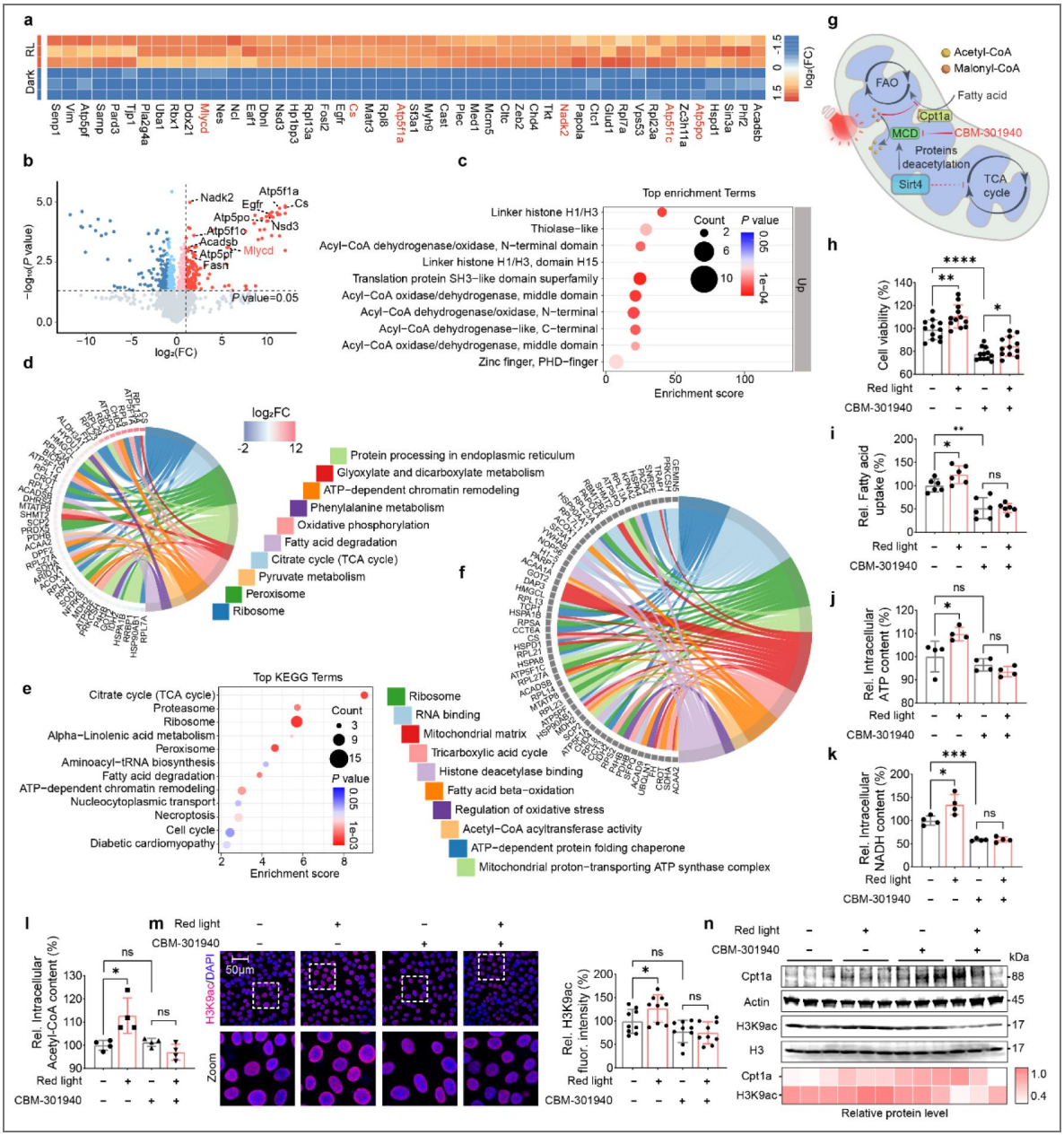

Figure 6. Red light activates lipid metabolism and increase H3K9ac levels in keratinocytes via SIRT4 downregulation-mediated MCD acetylation.

a, Heatmap showing the top 50 significantly differentially expressed acetylated proteins in red light-irradiated keratinocytes. **b,** Volcano plot of changes in the content of acetylation-modified proteins in keratinocytes after red light treatment. **c,** Acetylation modification proteomics top10 protein functional enrichment analysis (Protein functional annotation by InterPro). **d,** Proteomic top10 enriched pathway chordal map of red light irradiated keratinocytes (KEGG analysis). **e,** Top12 molecular process enriched by combined analysis of keratinocyte proteomics and acetylation modification proteomics after red light treatment (KEGG analysis). **f,** Top 10 pathways chordal map enriched by combined analysis of keratinocyte proteomics and acetylation modification proteomics after red light treatment. **g,** Schematic representation of the role of Sirt4 in mitochondria FAO and TCA cycle progress. **h, i, j, k** and **l,** Effects of red light on cell viability (CCK-8, **h**, n=12), fatty acid uptake (**i**, n=6), ATP production (**j**, n=4), NADH levels (**k**, n=4), and Acetyl-CoA content (**l**, n=4) in keratinocytes treated with 5 μM CBM-301940. **m** and **n,** Representative immunofluorescence staining of H3K9ac (**m**, n=9)and Western blot analysis of CPT1A, *β*-Actin, H3K9ac and H3 in keratinocytes treated with red light and 5 μM CBM-301940 (**n**, n=3).

of 10 cm, 51.04% of the red light fully penetrated the skin tissue (Fig S7c and d). This indicates that red light has a sufficient tissue penetration depth to reach the internal organs and tissues. Consequently, we assessed the SIRT4 protein expression levels in aged animal models. We observed that periodic red light treatment significantly reversed the upregulation of SIRT4 protein in central organs such as the liver, lungs, and kidneys of aged mice (Fig 7a-d). In contrast, the levels of H3k9ac increased significantly following red light exposure (Fig 7e-l). Fluorescence levels of p-NF-κB protein markedly decreased across all tissues and organs, indicating that periodic systemic red light irradiation not only alleviates inflammatory aging in skin tissue but also exerts anti-inflammatory effects on tissues and organs within its penetration depth range (Fig 7m-p). Additionally, we assessed P16 and LAMB1 protein expression levels, along with SASP inflammatory factor expression, in heart, liver, lung, and kidney tissues. Following periodic red light treatment, P16 protein expression decreased, whereas Lamin-B1 protein expression increased (Fig 7 m-p). The levels of most aging-associated SASP inflammatory factors significantly decreased after periodic red light treatment (Fig 7q-t). These findings further demonstrate, in an animal model, that periodic red light irradiation possesses tissue anti-aging effects.

In summary, our findings demonstrate that red light can reverse cellular senescence at both the cellular and tissue levels by downregulating SIRT4 protein expression. By elucidating the mechanism through which red light upregulates H3K9ac protein levels, we confirmed its potential role in mitigating cellular and tissue senescence by enhancing fatty acid oxidation and mitochondrial metabolism via SIRT4 downregulation, thereby increasing H3K9ac. We propose that SIRT4 protein downregulation represents a novel anti-aging intervention mechanism that activates mitochondrial and fatty acid metabolism to elevate H3K9ac levels and ultimately mitigate cellular aging. By controlling the abnormal age-related activation of SIRT4 during cellular aging processes and developing SIRT4 inhibitors, tissue-specific aging reversal and therapeutic interventions for metabolic-related diseases may be realized.

Discussion

The sirtuin family of proteins is also known as the longevity protein family[28]. The extensively documented SIRT1, SIRT3, and SIRT6 regulate various ageing-related pathways within cells by balancing the delicate equilibrium between cellular energy metabolism and protein acetylation modification through their NAD^+-dependent enzymatic activity, thereby exerting longevity-promoting effects[30, 51, 54–56]. Conversely, the function of mitochondrial-localized SIRT4 appears to oppose that of other sirtuins. Activation of SIRT4 protein inhibits fatty acid oxidation and mitochondrial metabolism and suppresses MAPK signalling activation[57, 58]. Following hepatic SIRT4 knockout, enhanced SIRT1 expression and restored PPAR-α-mediated lipid metabolism have been observed[53]. These studies suggest that the function of SIRT4 may inherently serve as a feedback regulatory mechanism for sirtuin family proteins, a conclusion corroborated by our findings. In our study, we observed that with advancing age, SIRT1 progressively diminished in the mouse skin stratum corneum, whereas SIRT4 levels intensified (Fig 5h). Periodic red light treatment reversed this expression pattern (Fig 5d-f), with red light-driven alterations in molecular and metabolic processes predominantly occurring within keratinocyte mitochondria. These findings further substantiate the potential mechanism by which red light irradiation modulates skin tissue anti-aging effects by regulating mitochondrial metabolism through SIRT4 protein levels.

Similarly, histone acetylation is closely linked to cellular metabolism[19]. H3K9ac, a typical transcriptional activation marker within the cellular genome, maintains active gene expression in young cells[59–61]. During aging, H3K9ac primarily drives cellular senescence through the combined effects of global loss and local abnormal accumulation[62]. On the one hand, as oxidative stress factors accumulate with age, functional suppression of acetyltransferases and declining mitochondrial function lead to reduced acetyl-CoA substrate levels[4]. Consequently, histone acetylation exhibits a characteristic global decline with age[20]. Conversely, senescent cells activate IKK by secreting inflammatory signals, such as TNF-α, which subsequently phosphorylates the P65

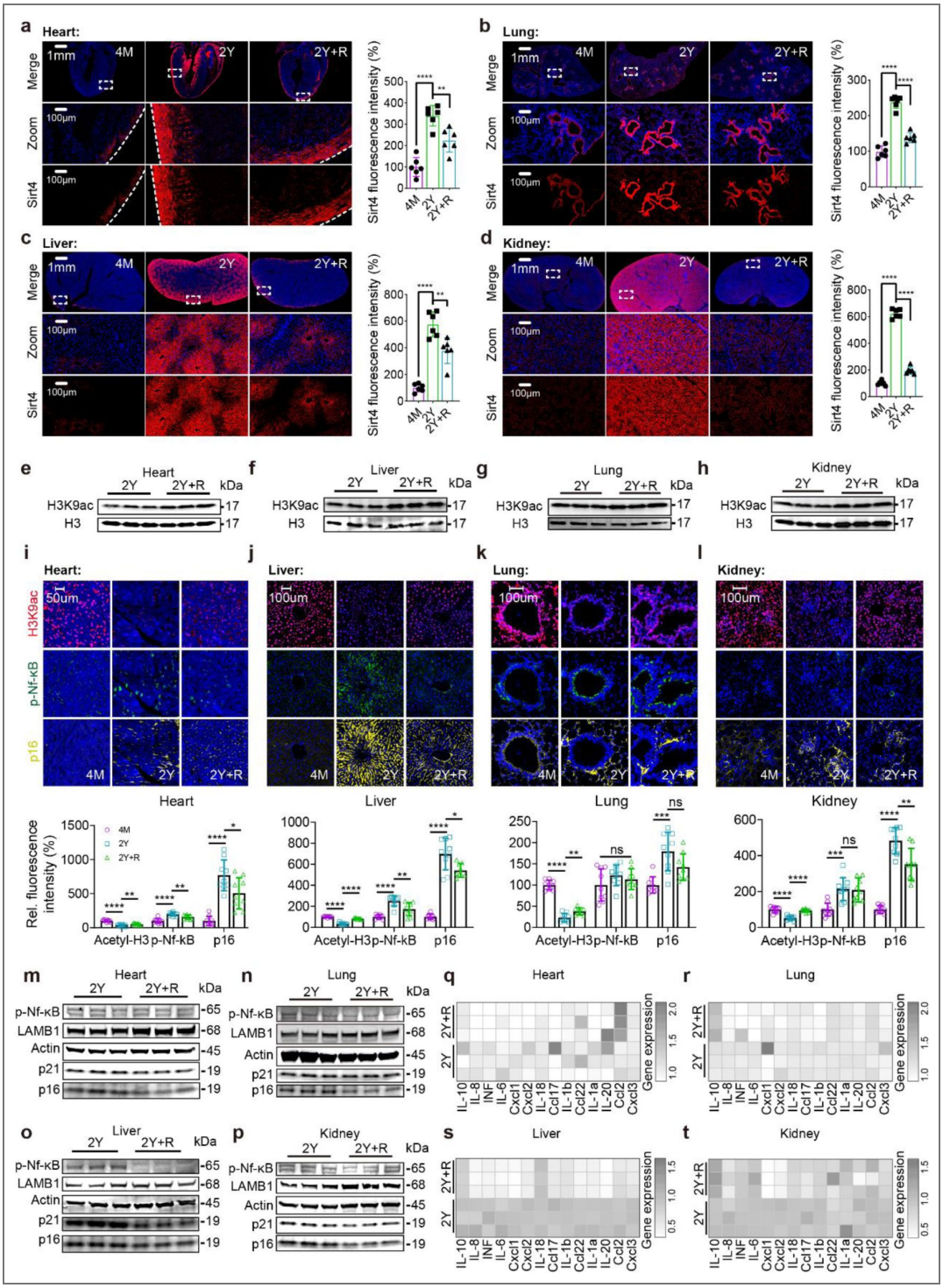

Figure 7. Inflammation and senescence signaling in aging model mice alleviated after cyclic treatment with red light.

a, b, c and **d,** Fluorescence images of Sirt4 (red) proteins in the heart (**a**), liver (**b**), lung (**c**)and kidney (**d**) of mice in groups 4M, 2Y and 2Y+R (DAPI, blue), n=6. **e, f, g** and **h,** The levels of H3K9ac proteins in the heart (**e**), liver (**f**), lung (**g**)and kidney (**h**) of mice in groups 4M, 2Y and 2Y+R, n=3. **i, j, k** and **l,** Fluorescence images of H3K9ac (Red), p-Nf-κB (green) and p16 (yellow) proteins in the heart (**i**), liver (**j**), lung (**k**)and kidney (**l**) of mice in groups 4M, 2Y and 2Y+R (DAPI, blue), n=6. **m, n, o** and **p,** The levels of p-Nf-κB, LAMB1, p21 and p16 proteins in the heart (**m**), liver (**n**), lung (**o**)and kidney (**p**) of mice in groups 4M, 2Y and 2Y+R, n=3. **q, r, s** and **t,** The expression heatmap of SASP inflammatory factors in the heart (**q**), liver (**r**), lung (**s**)and kidney (**t**) of mice in groups 4M, 2Y, and 2Y+R, n=3.

protein. This locally increases H3K9ac at the transcription sites of SASP inflammatory factors, such as IL-6 and IL-8, thereby driving the transcription of inflammatory molecules in senescent cells[63–66]. Our findings revealed that SIRT4 activates cellular metabolic processes, including fatty acid and TCA cycle metabolism, by deacetylating mitochondrial metabolism-related proteins, particularly MCD. Acetyl-CoA accumulated in SIRT4-downregulated cells (Fig 6). This SIRT4-mediated regulation of lipid metabolism partially restores overall H3K9ac levels in cells and tissues, as corroborated by experimental results at the animal tissue level. Furthermore, from the perspective of the antagonistic interaction between SIRT4 and SIRT1 proteins within cells, reduced SIRT4 levels restore SIRT1 protein expression in aged cells and tissues[67–69]. SIRT1 may exert anti-inflammatory effects through deacetylation of H3K9ac in the nucleolar region. Although the overall impact of SIRT4 downregulation on H3K9ac levels still manifests as increased acetylation at H3K9 sites in our findings, we observed a marked reduction in the expression of SASP inflammatory factors and mitigation of p-NF-κB-regulated inflammatory pathways in aged cells and tissues with diminished SIRT4 protein levels (Fig 7). These findings align with the established functions of SIRT1 in the nucleolar region. These findings demonstrate that in aging cells and tissues, red light irradiation-driven SIRT4 downregulation can reverse the gene expression pattern in senescent cells by simultaneously regulating the overall loss and nucleolar-localized accumulation of H3K9ac through a synergistic action with SIRT1. This restores cellular mitochondrial metabolic capacity and controls inflammatory bursts, demonstrating that SIRT4 has the potential to serve as a negative regulatory target for the modulation of aging.

Additionally, we observed that the most significant cellular change following red light irradiation of keratinocytes was a red light-driven metabolic alteration. We propose that this represents a novel avenue for investigating the biological and regulatory effects of red light. By examining its comprehensive impact on cellular metabolism, we can further elucidate the cellular regulatory mechanisms. This approach circumvents the complexity of the target diversity encountered in existing red-light research. Red light enters cells as an energy form[39, 70]. Through the conversion action of mitochondrial cytochrome oxidase, it transforms light energy into the driving force for maintaining a high mitochondrial membrane potential, thereby enhancing the efficiency of cellular mitochondrial function[71, 72]. Consequently, the levels of metabolic substrates within the cells are altered. We propose that this represents a triggering condition for red-light-mediated photobiomodulation in keratinocytes. Membrane potential-driven metabolism disrupts the relative equilibrium of metabolites within the cell. Metabolite-sensing systems are activated by detecting changes in key metabolite levels, subsequently regulating the activation of relevant metabolic pathways[58, 73, 74]. In contrast, the levels of various intracellular metabolites not only maintain the balance of cellular energy supply but also serve as dynamic markers that initiate protein ubiquitination and degradation pathways, which are crucial for maintaining intracellular protein homeostasis[75]. For instance, the oxidation modification of protein methionine/cysteine induced during metabolic activation disrupts protein structural homeostasis, exposing specific binding sites for ubiquitin E3 ligases, thereby mediating protein ubiquitination and degradation[76]. Furthermore, glycosylation modifications can regulate protein stability by competing with phosphorylation sites[77]. This suggests that red light may influence ubiquitin-dependent degradation of SIRT4 protein by modulating metabolism and metabolite levels. However, this mechanism requires further investigation to explain why red light reduces intracellular SIRT4 levels.

In summary, our study reports novel red-light-mediated cellular and tissue metabolic regulation and anti-aging effects by modulating the levels of the non-photosensitive protein SIRT4. The reduction in SIRT4 protein levels releases mitochondrial metabolic suppression in senescent cells, restores lipid metabolism regulated by PPAR-α, and further increases acetylation levels at senescence-associated histone acetylation sites. This mechanism underlies the regulatory effects of red light on senescent cells and tissues. Our findings elucidate the mechanism by which visible red light exerts anti-aging biological regulatory effects, distinguishing it from other sirtuin family members. Identifying SIRT4 inhibitors to control its elevated expression and activation in aging tissues holds promise as a novel anti-aging therapeutic approach. This study provides a clear molecular target and theoretical guidance for the further development of anti-skin aging products.

Data availability

All data are available in the main text or the Supplementary Materials. Original gel images of the western blots used in this study are shown in Supplementary Figs. 8-9. The RNA sequencing data related to this study has been deposited into the Sequence Read Archive (SRA) database, with accession code *http://www.ncbi.nlm.nih.gov/bioproject/1161480*. The Proteomics data and Acetylated proteomics data related to this study has been deposited into the The Genome Sequence Archive (GSA) database, with accession code *https://ngdc.cncb.ac.cn/omix/release/OMIX011505* and *https://ngdc.cncb.ac.cn/omix/release/OMIX011504*.

Acknowledgements

This work was supported by the National Natural Science Foundation of China (31971315) and the Postdoctoral Science Foundation of China (2024M754229). We are also grateful to Wu Si for her substantial support of this research.

Additional information

Author contributions

Fangqing Deng: design, acquisition of data, analysis and interpretation of data conceptualization, review & editing, methodology, investigation, data curation, and writing—original draft. Yingchun Yang and Zhaoxiang Yu: resources and writing–reviewing. Xu Li, Zibo Gao, Lihua Yang, Huifang Liu, Rong Yang, Monian Wang, Yang Liu, Jinyun Niu: investigation. Lianbing Zhang: conceptualization, review & editing, funding acquisition, resources, and supervision.

Funding

Funder	Grant reference number	Author
The National Natural Science Foundation of China	31971315	Lianbing Zhang
The Postdoctoral Science Foundation of China	2024M754229	Yingchun Yang

Author ORCID iDs

Lianbing Zhang: https://orcid.org/0000-0001-7803-6028

Additional files

Supplementary file 1.

References

1. **Ovadya Y.,** et al. (2018) Impaired immune surveillance accelerates accumulation of senescent cells and aging. *Nature Communications* **9** https://doi.org/10.1038/s41467-018-07825-3 | PubMed
2. **Jin C.,** et al. (2025) Molecular and genetic insights into human ovarian aging from single-nuclei multi-omics analyses. *Nat Aging* **5**:275-290 https://doi.org/10.1038/s43587-024-00762-5 | PubMed
3. **McClintock M.K.,** Dale W., Laumann E.O., Waite L. (2016) Empirical redefinition of comprehensive health and well-being in the older adults of the United States. *Proceedings of the National Academy of Sciences of the United States of America* **113**:E3071-E3080 https://doi.org/10.1073/pnas.1514968113 | PubMed
4. **Peleg S.,** Feller C., Ladurner A.G., Imhof A. (2016) The Metabolic Impact on Histone Acetylation and Transcription in Ageing. *Trends in Biochemical Sciences* **41**:700-711 https://doi.org/10.1016/j.tibs.2016.05.008 | PubMed

5. **Chen W.,** et al. (2021) The SESAME complex regulates cell senescence through the generation of acetyl-CoA. *Nature Metabolism* **3**:983-999 https://doi.org/10.1038/s42255-021-00412-9 | PubMed

6. **Dang W.W.,** et al. (2009) Histone H4 lysine 16 acetylation regulates cellular lifespan. *Nature* **459**:802-807 https://doi.org/10.1038/nature08085 | PubMed

7. **Yang Y.,** et al. (2022) Curcumin protects against manganese-induced neurotoxicity in rat by regulating oxidative stress-related gene expression via H3K27 acetylation. *Ecotoxicology and Environmental Safety* **236** https://doi.org/10.1016/j.ecoenv.2022.113469 | PubMed

8. **Wang Y.,** et al. (2025) Endometrial aging is accompanied by H3K27ac and PGR loss. *Nat Aging* **5**:816-830 https://doi.org/10.1038/s43587-025-00859-5 | PubMed

9. **Hitchiler M.J.,** Oberley L.W., Domann F.E. (2008) Epigenetic silencing of *SOD2* by histone modifications in human breast cancer cells. *Free Radical Biology and Medicine* **45**:1573-1580 https://doi.org/10.1016/j.freeradbiomed.2008.09.005 | PubMed

10. **Lu Y.F.,** et al. (2019) Increased acetylation of H3K14 in the genomic regions that encode trained immunity enzymes in lysophosphatidylcholine-activated human aortic endothelial cells - Novel qualification markers for chronic disease risk factors and conditional DAMPs. *Redox Biology* **24** https://doi.org/10.1016/j.redox.2019.101221 | PubMed

11. **Qu Q.,** et al. (2024) Lithocholic acid binds TULP3 to activate sirtuins and AMPK to slow down ageing. *Nature* https://doi.org/10.1038/s41586-024-08348-2 | PubMed

12. **Wang W.B.,** Pan K.W., Chen Y.F., Huang C.Y., Zhang X.W. (2012) The acetylation of transcription factor HBP1 by p300/CBP enhances $p16^{INK4}$ Aexpression. *Nucleic Acids Research* **40**:981-995 https://doi.org/10.1093/nar/gkr818 | PubMed

13. **Zhou R.,** Han L.M., Li G.D., Tong T.J. (2009) Senescence delay and repression of $p16^{INK4a}$ by Lsh via recruitment of histone deacetylases in human diploid fibroblasts. *Nucleic Acids Research* **37**:5183-5196 https://doi.org/10.1093/nar/gkp533 | PubMed

14. **Chen Y.X.,** et al. (2004) Histone acetylation regulates $p21^{WAF1}$ expression in human colon cancer cell lines. *World Journal of Gastroenterology* **10**:2643-2646 https://doi.org/10.3748/wjg.v10.i18.2643 | PubMed

15. **Pietrocola F.,** Galluzzi L., Bravo-San Pedro J.M., Madeo F., Kroemer G. (2015) Acetyl Coenzyme A: A Central Metabolite and Second Messenger. *Cell Metabolism* **21**:805-821 https://doi.org/10.1016/j.cmet.2015.05.014 | PubMed

16. **Bradshaw P.C.** (2021) Acetyl-CoA Metabolism and Histone Acetylation in the Regulation of Aging and Lifespan. *Antioxidants* **10** https://doi.org/10.3390/antiox10040572 | PubMed

17. **Kaelin W.G.,** McKnight S.L. (2013) Influence of Metabolism on Epigenetics and Disease. *Cell* **153**:56-69 https://doi.org/10.1016/j.cell.2013.03.004 | PubMed

18. **Yu R.F.,** et al. (2021) Inactivating histone deacetylase HDA promotes longevity by mobilizing trehalose metabolism. *Nature Communications* **12** https://doi.org/10.1038/s41467-021-22257-2 | PubMed

19. **Lu C.,** Thompson C.B. (2012) Metabolic Regulation of Epigenetics. *Cell Metabolism* **16**:9-17 https://doi.org/10.1016/j.cmet.2012.06.001 | PubMed

20. **Yang J.H.,** et al. (2023) Loss of epigenetic information as a cause of mammalian aging. *Cell* **186**:305-326 https://doi.org/10.1016/j.cell.2022.12.027 | PubMed

21. **Li P.,** Ge J., Li H. (2020) Lysine acetyltransferases and lysine deacetylases as targets for cardiovascular disease. *Nature Reviews Cardiology* **17**:96-115 https://doi.org/10.1038/s41569-019-0235-9 | PubMed

22. **Moreno-Yruela C.,** et al. (2022) Class I histone deacetylases (HDAC1-3) are histone lysine delactylases. *Science Advances* **8** https://doi.org/10.1126/sciadv.abi6696 | PubMed

23. **Yang X.J.** (2004) The diverse superfamily of lysine acetyltransferases and their roles in leukemia and other diseases. *Nucleic Acids Res* **32**:959-976 https://doi.org/10.1093/nar/gkh252 | PubMed

24. **Guerriero J.L.,** et al. (2017) Class IIa HDAC inhibition reduces breast tumours and metastases through anti-tumour macrophages. *Nature* **543**:428-432 https://doi.org/10.1038/nature21409 | PubMed

25. **Wellman A.S.,** et al. (2017) Intestinal Epithelial Sirtuin 1 Regulates Intestinal Inflammation During Aging in Mice by Altering the Intestinal Microbiota. *Gastroenterology* **153**:772-786 https://doi.org/10.1053/j.gastro.2017.05.022 | PubMed

26. **Karamanlidis G.,** et al. (2013) Mitochondrial Complex I Deficiency Increases Protein Acetylation and Accelerates Heart Failure. *Cell Metabolism* **18**:239-250 https://doi.org/10.1016/j.cmet.2013.07.002 | PubMed

27. **Imai S.-i.,** Guarente L. (2014) NAD^+ and sirtuins in aging and disease. *Trends in Cell Biology* **24**:464-471 https://doi.org/10.1016/j.tcb.2014.04.002 | PubMed

28. **Chen M.K.,** et al. (2024) Research progress on Sirtuins (SIRTs) family modulators. *Biomedicine & Pharmacotherapy* **174** https://doi.org/10.1016/j.biopha.2024.116481 | PubMed

29. **Cao D.Y.,** Bai G., Ji Y.P., Traub R.J. (2015) Epigenetic upregulation of metabotropic glutamate receptor 2 in the spinal cord attenuates oestrogen-induced visceral hypersensitivity. *Gut* **64**:1913-1920 https://doi.org/10.1136/gutjnl-2014-307748 | PubMed

30. **Watroba M.,** Szukiewicz D. (2016) The role of sirtuins in aging and age-related diseases. *Advances in Medical Sciences* **61**:52-62 https://doi.org/10.1016/j.advms.2015.09.003 | PubMed

31. **Yang Y.H.,** et al. (2007) SIRT1 sumoylation regulates its deacetylase activity and cellular response to genotoxic stress. *Nature Cell Biology* **9**:1253-U1280 https://doi.org/10.1038/ncb1645 | PubMed

32. **Shinmura K.** (2013) Effects of Caloric Restriction on Cardiac Oxidative Stress and Mitochondrial Bioenergetics: Potential Role of Cardiac Sirtuins. *Oxidative Medicine and Cellular Longevity* **2013** https://doi.org/10.1155/2013/528935 | PubMed

33. **Ji Z.,** Liu G.-H., Qu J. (2022) Mitochondrial sirtuins, metabolism, and aging. *Journal of Genetics and Genomics* **49**:287-298 https://doi.org/10.1016/j.jgg.2021.11.005 | PubMed

34. **Pezzotta A.,** et al. (2022) Low Nephron Number Induced by Maternal Protein Restriction Is Prevented by Nicotinamide Riboside Supplementation Depending on Sirtuin 3 Activation. *Cells* **11** https://doi.org/10.3390/cells11203316 | PubMed

35. **Balough J.L.,** Dipali S.S., Velez K., Kumar T.R., Duncan F.E. (2024) Hallmarks of female reproductive aging in physiologic aging mice. *Nature Aging* **4**:1711-1730 https://doi.org/10.1038/s43587-024-00769-y | PubMed

36. **Xie N.,** et al. (2020) NAD^+ metabolism: pathophysiologic mechanisms and therapeutic potential. *Signal Transduction and Targeted Therapy* **5** https://doi.org/10.1038/s41392-020-00311-7 | PubMed

37. **Zhang G.,** et al. (2022) Photobiomodulation promotes angiogenesis in wound healing through stimulating the nuclear translocation of VEGFR2 and STAT3. *Journal of Photochemistry and Photobiology B-Biology* **237** https://doi.org/10.1016/j.jphotobiol.2022.112573 | PubMed

38. **Deng F.Q.,** et al. (2024) Visible light accelerates skin wound healing and alleviates scar formation in mice by adjusting STAT3 signaling. *Communications Biology* **7** https://doi.org/10.1038/s42003-024-06973-1 | PubMed

39. **Cios A.,** et al. (2021) Effect of Different Wavelengths of Laser Irradiation on the Skin Cells. *International Journal of Molecular Sciences* **22** https://doi.org/10.3390/ijms22052437 | PubMed

40. **Kim H.,** et al. (2022) Benefits of a Skull-Interfaced Flexible and Implantable Multilight Emitting Diode Array for Photobiomodulation in Ischemic Stroke. *Advanced Science* **9** https://doi.org/10.1002/advs.202104629 | PubMed

41. **Yoon J.S.,** Ku W.Y., Lee J.H., Ahn H.C. (2020) Low-level light therapy using a helmet-type device for the treatment of androgenetic alopecia A 16-week, multicenter, randomized, double-blind, sham device-controlled trial. *Medicine* **99** https://doi.org/10.1097/md.0000000000021181 | PubMed

42. **Kent A.L.,** et al. (2020) A pilot randomised clinical trial of 670 nm red light for reducing retinopathy of prematurity. *Pediatric Research* **87**:131-136 https://doi.org/10.1038/s41390-019-0520-7 | PubMed

43. **Li M.,** et al. (2024) A wearable and stretchable dual-wavelength LED device for home care of chronic infected wounds. *Nature Communications* **15** https://doi.org/10.1038/s41467-024-53579-6 | PubMed

44. **Hui J.,** et al. (2025) Low-Irradiance Antimicrobial Blue Light-Bathing Therapy for Wound Infection Control. *Advanced Science* **12** https://doi.org/10.1002/advs.202412493 | PubMed

45. **Yang L.D.,** et al. (2022) Non-invasive photobiomodulation treatment in an Alzheimer Disease-like transgenic rat model. *Theranostics* **12**:2205-2231 https://doi.org/10.7150/thno.70756 | PubMed

46. **López-Otín C.,** Blasco M.A., Partridge L., Serrano M., Kroemer G. (2023) Hallmarks of aging: An expanding universe. *Cell* **186**:243-278 https://doi.org/10.1016/j.cell.2022.11.001 | PubMed

47. **Oh S.,** et al. (2022) Combined Treatment of Monopolar and Bipolar Radiofrequency Increases Skin Elasticity by Decreasing the Accumulation of Advanced Glycated End Products in Aged Animal Skin. *International Journal of Molecular Sciences* **23** https://doi.org/10.3390/ijms23062993 | PubMed

48. **Wunsch A.,** Matuschka K. (2014) A Controlled Trial to Determine the Efficacy of Red and Near-Infrared Light Treatment in Patient Satisfaction, Reduction of Fine Lines, Wrinkles, Skin Roughness, and Intradermal Collagen Density Increase. *Photomedicine and Laser Surgery* **32**:93-100 https://doi.org/10.1089/pho.2013.3616 | PubMed

49. **Gao X.L.,** et al. (2022) Photobiomodulation Drives MiR-136-5p Expression to Promote Injury Repair after Myocardial Infarction. *International Journal of Biological Sciences* **18**:2980-2993 https://doi.org/10.7150/ijbs.71440 | PubMed

50. **Hamblin M.R.** (2018) Mechanisms and Mitochondrial Redox Signaling in Photobiomodulation. *Photochemistry and Photobiology* **94**:199-212 https://doi.org/10.1111/php.12864 | PubMed

51. **Chen H.H.,** et al. (2023) Role of sirtuins in metabolic disease-related renal injury. *Biomedicine & Pharmacotherapy* **161** https://doi.org/10.1016/j.biopha.2023.114417 | PubMed

52. **Laurent G.,** et al. (2013) SIRT4 coordinates the balance between lipid synthesis and catabolism by repressing malonyl CoA decarboxylase. *Mol Cell* **50**:686-698 https://doi.org/10.1016/j.molcel.2013.05.012 | PubMed

53. **Laurent G.,** et al. (2013) SIRT4 represses peroxisome proliferator-activated receptor α activity to suppress hepatic fat oxidation. *Mol Cell Biol* **33**:4552-4561 https://doi.org/10.1128/mcb.00087-13 | PubMed

54. **Singh C.K.,** et al. (2018) The Role of Sirtuins in Antioxidant and Redox Signaling. *Antioxidants & Redox Signaling* **28**:643-661 https://doi.org/10.1089/ars.2017.7290 | PubMed

55. **Higgins C.B.,** et al. (2022) SIRT1 selectively exerts the metabolic protective effects of hepatocyte nicotinamide phosphoribosyltransferase. *Nature Communications* **13** https://doi.org/10.1038/s41467-022-28717-7 | PubMed

56. **Chang H.-C.,** Guarente L. (2014) SIRT1 and other sirtuins in metabolism. *Trends in Endocrinology and Metabolism* **25**:138-145 https://doi.org/10.1016/j.tem.2013.12.001 | PubMed

57. **Rehan M.,** et al. (2021) Restoration of SIRT3 gene expression by airway delivery resolves age-associated persistent lung fibrosis in mice. *Nature Aging* **1**:205-217 https://doi.org/10.1038/s43587-021-00027-5 | PubMed

58. **Hardie D.G.,** Ross F.A., Hawley S.A. (2012) AMPK: a nutrient and energy sensor that maintains energy homeostasis. *Nature Reviews Molecular Cell Biology* **13**:251-262 https://doi.org/10.1038/nrm3311 | PubMed

59. **Sen P.,** Shah P.P., Nativio R., Berger S.L. (2016) Epigenetic Mechanisms of Longevity and Aging. *Cell* **166**:822-839 https://doi.org/10.1016/j.cell.2016.07.050 | PubMed

60. **Camillo L.P.D.,** Asif M.H., Horvath S., Larschan E., Singh R. (2025) Histone mark age of human tissues and cell types. *Science Advances* **11** https://doi.org/10.1126/sciadv.adk9373 | PubMed

61. **Klein H.U.,** et al. (2019) Epigenome-wide study uncovers large-scale changes in histone acetylation driven by tau pathology in aging and Alzheimer's human brains. *Nature Neuroscience* **22**:37-46 https://doi.org/10.1038/s41593-018-0291-1 | PubMed

62. **Jasiulionis M.G.** (2018) Abnormal Epigenetic Regulation of Immune System during Aging. *Frontiers in Immunology* **9** https://doi.org/10.3389/fimmu.2018.00197 | PubMed

63. **Vandenbon A.,** Kumagai Y., Lin M.J., Suzuki Y., Nakai K. (2018) Waves of chromatin modifications in mouse dendritic cells in response to LPS stimulation. *Genome Biology* **19** https://doi.org/10.1186/s13059-018-1524-z | PubMed

64. **Hu L.L.,** et al. (2017) Epigenetic Regulation of Interleukin 6 by Histone Acetylation in Macrophages and Its Role in Paraquat-Induced Pulmonary Fibrosis. *Frontiers in Immunology* **7** https://doi.org/10.3389/fimmu.2016.00696 | PubMed

65. **Chang H.C.,** Guarente L. (2013) SIRT1 Mediates Central Circadian Control in the SCN by a Mechanism that Decays with Aging. *Cell* **153**:1448-1460 https://doi.org/10.1016/j.cell.2013.05.027 | PubMed

66. **Adamkova K.,** et al. (2017) SIRT1-dependent modulation of methylation and acetylation of histone H3 on lysine 9 (H3K9) in the zygotic pronuclei improves porcine embryo development. *Journal of Animal Science and Biotechnology* **8** https://doi.org/10.1186/s40104-017-0214-0 | PubMed

67. **Min Z.Y.,** Gao J.M., Yu Y. (2019) The Roles of Mitochondrial SIRT4 in Cellular Metabolism. *Frontiers in Endocrinology* **9** https://doi.org/10.3389/fendo.2018.00783 | PubMed

68. **Mehrabipour M.,** et al. (2024) SIRT4 as a novel interactor and candidate suppressor of C-RAF kinase in MAPK signaling. *Life Sci Alliance* **7** https://doi.org/10.26508/lsa.202302507 | PubMed

69. **Tang B.L.** (2016) Sirt1 and the Mitochondria. *Molecules and Cells* **39**:87-95 https://doi.org/10.14348/molcells.2016.2318 | PubMed

70. **Young A.R.** (1997) Chromophores in human skin. *Phys Med Biol* **42**:789-802 https://doi.org/10.1088/0031-9155/42/5/004 | PubMed

71. **Fuchs C.,** et al. (2021) Photobiomodulation Response From 660 nm is Different and More Durable Than That From 980 nm. *Lasers Surg Med* **53**:1279-1293 https://doi.org/10.1002/lsm.23419 | PubMed

72. **Lunova M.,** et al. (2020) Light-induced modulation of the mitochondrial respiratory chain activity: possibilities and limitations. *Cell Mol Life Sci* **77**:2815-2838 https://doi.org/10.1007/s00018-019-03321-z | PubMed

73. **Saxton R.A.,** Sabatini D.M. (2017) mTOR Signaling in Growth, Metabolism, and Disease. *Cell* **168**:960-976 https://doi.org/10.1016/j.cell.2017.02.004 | PubMed

74. **Kim J.,** Guan K.L. (2019) mTOR as a central hub of nutrient signalling and cell growth. *Nat Cell Biol* **21**:63-71 https://doi.org/10.1038/s41556-018-0205-1 | PubMed

75. **Ciechanover A.** (1998) The ubiquitin-proteasome pathway: on protein death and cell life. *Embo Journal* **17**:7151-7160 https://doi.org/10.1093/emboj/17.24.7151 | PubMed

76. **Zhang Y.,** et al. (2025) The emerging role of E3 ubiquitin ligases and deubiquitinases in metabolic dysfunction-associated steatotic liver disease. *Journal of Translational Medicine* **23** https://doi.org/10.1186/s12967-025-06255-2 | PubMed

77. **Gu X.,** et al. (2025) O-GlcNAcylation-Ubiquitin Crosstalk of METTL1 Drives m7G Epitranscriptomic Collapse and Lipid Metabolic Reprogramming in Diabetic Cardiomyopathy. *bioRxiv* https://doi.org/10.1101/2025.07.07.663452

Fangqing Deng (2025) Proteomic and acetylated modified proteomic analysis of keratinocytes treated with red light irradiation-1. National Genomics Data Center (NGDC). ID OMIX011505 https://ngdc.cncb.ac.cn/omix/release/OMIX011505

Fangqing Deng (2025) Proteomic and acetylated modified proteomic analysis of keratinocytes treated with red light irradiation-2. National Genomics Data Center (NGDC). ID OMIX011504 https://ngdc.cncb.ac.cn/omix/release/OMIX011504

Fangqing Deng (2024) Raw data of Red and blue light irradiates keratinocytes. Sequence Read Archive (SRA). ID 1161480 http://www.ncbi.nlm.nih.gov/bioproject/1161480

Peer reviews

Reviewer #1 (Public review):

Summary:

Deng and colleagues pursue the possibility that red light exposure can provide some benefits and anti-senescence effects in aged mouse models. In addition, they show how red light influences metabolism in cultured keratinocytes. The authors provide a long dissection of the potential paths involved in the changes promoted by red light exposure, identifying CytC oxidase, SIRT4, PPARa and MCD as key players.

Strengths:

The authors did a thorough exploration of the multiple potential avenues by which red light exposure influences metabolism. The in vitro and in vivo evidence nicely complement each other.

Weaknesses:

This is a challenging hypothesis that would require some additional experimental controls. The pathway dissection, while extensive, is sometimes approached in unconvincing ways, and the results are not always evident to judge or interpret. Technically, the western blots and transcriptomic analyses require notable improvements.

https://doi.org/10.7554/eLife.111498.1.sa2

Reviewer #2 (Public review):

Summary:

This work identifies a previously unknown way that red light can slow ageing. The authors show that red light lowers the level of a protein called SIRT4 in skin cells. Reducing SIRT4 boosts fatty acid use and increases a type of histone modification that keeps genes active. These changes help cells clear away signs of ageing, reduce inflammation, and restore normal metabolism. The findings open the possibility of developing new treatments that target SIRT4 to reverse age-related decline.

Strengths:

The evidence is solid because the authors use several complementary methods. They test red light in both cultured cells and naturally aged mice, and they confirm the key role of SIRT4 by silencing its gene. Measurements of metabolism, protein changes, and ageing markers all point in the same direction. However, the exact way red light lowers SIRT4 levels is not fully explained, which leaves a minor gap. Overall, the conclusions are well supported and convincing.

Weaknesses:

The paper does not evolve to use the mechanistic discoveries of the manuscript to help our community to identify the mechanism of photobiomodulation, which is not known so far.

I would like to draw attention to a recently published paper by Herrera et al. (FEBS Letters 2025, doi:10.1002/1873-3468.70195), which shows that red light (660 nm) stimulates mitochondrial fatty acid oxidation in keratinocytes via AMPK-dependent phosphorylation of ACC, without altering expression of electron transport chain complexes. I believe this paper is highly complementary to the current study.

Herrera et al. demonstrate that red light increases basal, ATP-linked, and maximal oxygen consumption rates in keratinocytes specifically through enhanced fatty acid oxidation (inhibited by etomoxir). This independently validates the central finding of the current manuscript, i.e., red light boosts lipid metabolism, strengthening the robustness of this concept.

While the current manuscript focuses on the SIRT4-MCD axis, Herrera et al. identify AMPK phosphorylation and ACC inhibition as key effectors. The authors can integrate and expand their discussion, since SIRT4 downregulation may converge on AMPK activation, or they may represent parallel, reinforcing mechanisms. This would enrich the mechanistic model and open new hypotheses.

The mechanism of photobiomodulation: Herrera et al. explicitly challenge the prevailing paradigm that red light acts solely via cytochrome c oxidase (by showing long-lasting effects, unchanged OXPHOS protein levels, and no difference in permeabilised cells). The current finding (red light acts through SIRT4 downregulation, i.e., not direct enzymatic activation) aligns perfectly with Herreraś critique.

Long-term metabolic effects - Herrera et al. show that a single red light exposure elevates oxygen consumption for up to 2 days. The current study focuses on changes at 12-24 h. Their data extend the time window and suggest that the metabolic reprogramming you describe may persist longer than currently discussed, which is clinically relevant.

Discussing Herrera et al.'s results would not only acknowledge independent, corroborating evidence but would also allow the authors to position their SIRT4-centric mechanism within a broader, emerging understanding of red-light photobiomodulation.

https://doi.org/10.7554/eLife.111498.1.sa1

Author response:

> ***Reviewer #1 (Public review):***
>
> *Weaknesses:*
>
> *This is a challenging hypothesis that would require some additional experimental controls. The pathway dissection, while extensive, is sometimes approached in unconvincing ways, and the results are not always evident to judge or interpret. Technically, the western blots and transcriptomic analyses require notable improvements.*

We would like to thank the reviewer for the careful and patient examination of the issues identified in our manuscript. The poor quality of some of the Western blot bands in Figure 4 may have been caused by inappropriate electrophoresis conditions during the Western blot experiments. In the revised manuscript, we will optimize the electrophoresis conditions to obtain higher-quality protein bands and update the quantitative data. Regarding the quantification format, we believe that heatmaps provide a more intuitive representation of trends in protein expression across different treatment groups. This approach more accurately reflects the results of our biological replicates than simply analyzing the significance of differences in the grayscale values of protein bands. For the analysis of transcriptomic data, we will conduct a more detailed analysis of signal pathway enrichment and the identified differentially expressed genes to ensure that predicted genes are excluded from our current results and redundant data presentation is removed.

Regarding additional experimental controls, such as incorporating experimental data under blue light treatment conditions as a control for red light. While exploring the optimal red light irradiation dose at the cellular level, we simultaneously conducted experiments on the

effects of blue light irradiation at the same dose on keratinocyte activity. The results indicated that as the blue light irradiation dose increased (0–160 J/cm^2), the keratinocyte activity exhibited a dose-dependent decline. This indicates that blue light is phototoxic to keratinocytes. The relevant experimental results have already been published in our previous study (Communications Biology 2024, doi: 10.1038/s42003-024-06973-1). Taken together with the data from our study, this demonstrates that the anti-aging effects of red light reported in the current manuscript are indeed driven by red light.

> ***Reviewer #2 (Public review):***
>
> *Weaknesses:*
>
> *The paper does not evolve to use the mechanistic discoveries of the manuscript to help our community to identify the mechanism of photobiomodulation, which is not known so far.*
>
> *I would like to draw attention to a recently published paper by Herrera et al. (FEBS Letters 2025, doi:10.1002/1873-3468.70195), which shows that red light (660 nm) stimulates mitochondrial fatty acid oxidation in keratinocytes via AMPK-dependent phosphorylation of ACC, without altering expression of electron transport chain complexes. I believe this paper is highly complementary to the current study.*
>
> *Herrera et al. demonstrate that red light increases basal, ATP-linked, and maximal oxygen consumption rates in keratinocytes specifically through enhanced fatty acid oxidation (inhibited by etomoxir). This independently validates the central finding of the current manuscript, i.e., red light boosts lipid metabolism, strengthening the robustness of this concept.*
>
> *While the current manuscript focuses on the SIRT4-MCD axis, Herrera et al. identify AMPK phosphorylation and ACC inhibition as key effectors. The authors can integrate and expand their discussion, since SIRT4 downregulation may converge on AMPK activation, or they may represent parallel, reinforcing mechanisms. This would enrich the mechanistic model and open new hypotheses.*
>
> *The mechanism of photobiomodulation: Herrera et al. explicitly challenge the prevailing paradigm that red light acts solely via cytochrome c oxidase (by showing long-lasting effects, unchanged OXPHOS protein levels, and no difference in permeabilised cells). The current finding (red light acts through SIRT4 downregulation, i.e., not direct enzymatic activation) aligns perfectly with Herreraś critique.*
>
> *Long-term metabolic effects-Herrera et al. show that a single red light exposure elevates oxygen consumption for up to 2 days. The current study focuses on changes at 12-24 h. Their data extend the time window and suggest that the metabolic reprogramming you describe may persist longer than currently discussed, which is clinically relevant.*
>
> *Discussing Herrera et al.'s results would not only acknowledge independent, corroborating evidence but would also allow the authors to position their SIRT4-centric mechanism within a broader, emerging understanding of red-light photobiomodulation.*

We would like to thank the reviewer for providing us with constructive suggestions for discussion. Our results showed that under red light conditions, both glycolipid and lipid metabolism were activated in keratinocytes, and cellular metabolic flux increased. The activation of lipid metabolism directly led to an increase in metabolism-associated H3K9ac and drove the upregulation of anti-aging-related genes; we believe this is key to the anti-aging effects of red light. Mechanistic analysis combining proteomics and acetylation proteomics revealed that red light significantly downregulated SIRT4 expression and increased the acetylation of MCD, a protein regulated by SIRT4 that governs cellular fatty acid oxidation

rates. Through validation using cell-level knockdown and inhibitors, we confirmed that SIRT4 inhibition exerts anti-aging effects *in vitro* and that inhibiting MCD function under red light conditions suppresses H3K9ac. These results establish the role of the SIRT4-MCD signalling axis in mediating the anti-aging effects of red light.

The study by Herrera et al. included a substantial body of validation data confirming the role of red light in promoting fatty acid oxidation, providing robust empirical support for our research. Furthermore, Herrera et al. revealed that red light-induced fatty acid oxidation depends on AMPK and ACC phosphorylation. This mechanism of red-light photobiomodulation may refute the notion that its bio-regulatory effects rely solely on the action of mitochondrial cytochrome c oxidase. Furthermore, together with our study revealing that red light exerts anti-aging photobiomodulatory effects via the SIRT4-MCD signalling axis, these findings independently confirm that red light regulates cellular fatty acid oxidation, thereby demonstrating the pivotal role of activated fatty acid oxidation in the bio-regulatory effects of red light. In the revised manuscript, we will include a discussion on the potential link between the red light-driven downregulation of SIRT4 and the phosphorylation of AMPK/ACC. This will be of positive value in elucidating how SIRT4 exerts its anti-aging effects by regulating lipid metabolism, as well as in explaining the possible mechanisms by which red light downregulates SIRT4.

https://doi.org/10.7554/eLife.111498.1.sa0